Numerical modelling of the effects of consolidation on the undrained spudcan capacity under combined loading in silty clay.

Manuscript resubmitted to *Computers and Geotechnics* on 5/12/2016 by:

Raffaele Ragni[1] (corresponding author)
Research Associate

Tel: +61 (0) 8 6488 7254
Email: 21358454@student.uwa.edu.au

Britta Bienen[1]
Senior Lecturer

Tel: +61 (0) 8 6488 4246
Email: britta.bienen@uwa.edu.au

Dong Wang[2]
Professor

Tel: +86 (0) 532 6678 6396
Email: dongwang@ouc.edu.cn

David Mašín[3]
Associate Professor

Tel: +420 2 2195 1552
Email: masin@natur.cuni.cz

Mark J. Cassidy[1]
Professor
Director

Tel: +61 (0) 8 6488 3732
Email: mark.cassidy@uwa.edu.au

[1] Centre for Offshore Foundation Systems and ARC CoE for Geotechnical Science and Engineering
University of Western Australia
35 Stirling Hwy, Crawley, Perth, WA 6009
Australia

[2] Shandong Provincial Key Laboratory of Marine Environment and Geological Engineering
Ocean University of China
238 Songling Street, Qingdao 266100
China

[3] Faculty of Science
Charles University in Prague
Albertov 3, 128 43 Praha
Czech Republic

ABSTRACT

The paper shows the increase in vertical and combined horizontal and moment bearing capacity of jack-up spudcan installed in silty clay, when a load-hold period is accounted for. The numerical implementation of a hypoplastic model for structured clays, combined with large deformation coupled analyses allowed the modelling of the spudcan installation process. Results were mapped into three-dimensional small strain analyses, conducted to investigate the combined loading capacity and describe the yield surface. The underlying failure mechanisms were investigated and increases in capacity due to consolidation determined. Experimental centrifuge data on carbonate silty clay validated the qualitative trend revealed numerically.

Keywords: Spudcan; Consolidation; Combined capacity; VHM; Numerical modelling; Hypoplasticity.

1. INTRODUCTION

Foundations for offshore jack-up platforms, also known as spudcans, are subjected to different loading conditions during their lifetime. The installation phase involves mainly vertical loading, as the installation is achieved by penetrating the spudcan into the soil under the self-weight of the structure and additional seawater ballast. Once in service, however, the spudcan is required to provide the necessary resistance to lateral and overturning loads which arise from metocean actions, such as waves, currents and wind (ISO 2012). For this reason, the combined bearing capacity under multi-directional vertical, horizontal and moment loading of the foundation must be demonstrated in a site-specific assessment.

Models that describe the interaction of vertical, horizontal and moment degrees-of-freedom in the resulting combined foundation capacity were first proposed by Roscoe & Schofield (1956), with the introduction of a yield surface concept. Further developments from Butterfield & Ticof (1979) and Schotman (1989) led to the first complete incremental force-resultant model based on plasticity theory for spudcan footings. Nova & Montrasio (1991) introduced the idea of macro-element to evaluate settlements and rotations of shallow foundations. The formulation of full macro-element models involves a yield surface to describe the combined bearing capacity of the footing in the vertical V, horizontal H and moment M loading space (VHM, Figure 1). Intuitively, the size of this surface is a function of the vertical load V, which in turn depends on the spudcan embedment w.

Dean et al. (1997), Cassidy & Houlsby (1999), Bienen et al. (2006) and Salciarini & Tamagnini (2009) proposed VHM force-resultant models for spudcans and shallow circular foundations in sand, where fully drained behaviour can be assumed. Martin & Houlsby (2000, 2001) and Zhang et al. (2011, 2013) focused instead on the response in clay, where undrained soil behaviour is observed. Models that describe the VHM capacity of foundations

with other geometries (strip, rectangular, skirted) have also been proposed (Bransby & Randolph 1998, Houlsby & Puzrin 1999, Gourvenec 2007).

An important aspect not considered in previous research is the consolidation that can take place in intermediate soils (i.e. silty soils that display intermediate drainage characteristics), as a consequence of excess pore pressure dissipation. This may occur during jack-up installation, as a consequence of pauses in leg penetration, and during the phase of operation, as the self-weight of the jack-up platform maintains a mean vertical stress on the foundation. Bienen & Cassidy (2013), Stanier et al. (2014), Bienen et al. (2015), Wang & Bienen (2016) and Ragni et al. (2016) demonstrated that maintaining the vertical load, or a fraction of it, on the spudcan for a certain time results in excess pore pressure dissipation around the spudcan, a reduction in void ratio and increased shear strength. A consequent V peak upon further penetration, following this consolidation phase, is schematically illustrated in Figure 1. Consolidation is expected to result in increases in the combined bearing capacity as well, though the improvement may not be uniform in all directions such that the yield surface may change shape as it expands. In the case of spudcan footings, the combined capacity will be tested under storm conditions. When considering the rate at which metocean actions are applied, the foundation response under *VHM* loading, even in intermediate soils, can be expected to be undrained.

This paper investigates the increase in undrained *VHM* capacity of a spudcan in silty clay following a period of consolidation under vertical load by means of numerical analyses. In contrast to most of the previous numerical analyses (Templeton et al. 2005, Templeton 2009, Zhang et al. 2011), where the footing was pre-embedded at a target depth with the soil undisturbed, the installation phase was modelled here prior to consolidation and determination of the *VHM* capacity. This therefore accounts for the remoulding effect and entrapment of soil under the spudcan during the initial installation.

2. NUMERICAL MODEL

An appropriate description of the problem as illustrated in Figure 1 requires first of all the modelling of spudcan penetration to a certain depth and the following consolidation stage. This involves large vertical penetration (here one footing diameter *D*, or 12 m, was chosen) and results in a high degree of shearing and remoulding in the soil. Therefore, a two-dimensional Large Deformation Finite Element (LDFE) approach was employed.

Secondly, the hypoplastic constitutive model for structured clays adopted was able to simulate the soil remoulding experienced in the large-amplitude penetration. The model was suitable for the full simulation of the installation, consolidation and the following undrained *VHM* loading, with the variations of excess pore pressures and void ratio captured.

Determination of the combined bearing capacity usually requires Small Strain Finite Element (SSFE) analyses only, given the small soil strains and consequent very limited mesh distortion, compared to the large deformation occurring during penetration. In contrast to the installation phase, which can be modelled using axisymmetry, determination of the combined *VHM* capacity requires a three-dimensional model. To account for the effects of installation, a rigorous mapping procedure of the soil properties and state variables is required, when passing from the axisymmetric LDFE model to the SSFE analyses.

The following sections explain in more detail the above mentioned characteristics of the numerical model.

2.1 Large deformation analyses of spudcan penetration and consolidation

The process of spudcan installation involves large deformations and results in a significant amount of straining and remoulding in the soil (Hossain et al. 2005, Yi et al. 2014, Zhang et al. 2014b, Hu et al. 2015), exceeding traditional small strain numerical analysis capabilities.

For this reason, this research adopted a Remeshing and Interpolation Technique with Small Strain (RITSS, Hu & Randolph 1998, Wang et al. 2015) strategy, where the entire penetration of the spudcan was divided into a sequence of multiple steps, each small enough to avoid excessive mesh distortion. At the end of each step, the distorted mesh was regenerated, while state variables and excess pore pressures are mapped from the previous step to the next. Once the target depth *w* was reached, the consolidation stage was performed by holding the load, or a fraction of it, for a given time. The same remeshing strategy was also applied within the consolidation stage when the accumulated settlement caused excessive mesh distortion. Simulation of coupled effective stress-pore fluid analyses was necessary to track the generation of excess pore pressures during penetration and following dissipation during consolidation.

Following this approach, Ragni et al. (2016) showed increases in vertical bearing capacity resulting from pauses in penetration, with the magnitude of such increments being proportional to the length of the consolidation phases (shown in Figure 5, which is discussed in the results section). As detailed in the following section, the numerical model took into account the effects of soil softening through the implementation of a variable called sensitivity; this revealed contrasting behaviours post-consolidation, either beneficial or detrimental for the stability of the structure, depending on the amount of sensitivity and its rate of degradation.

A thorough description of the effects of consolidation on spudcan penetration, modelled with RITSS analyses, can be found in Ragni et al. (2016) and Wang & Bienen (2016).

2.2 Hypoplastic constitutive model for structured clays

In contrast to conventional elasto-plasticity, where a clear distinction is made between elastic and plastic deformations, hypoplastic models introduce irreversible strains inside what is

known as the state boundary surface, for the elastic range is known to be extremely limited in soils. In the present work, an advanced hypoplastic constitutive model for clays was adopted, developed by Mašín (2014) and implemented in Abaqus/Standard as an updated version of the user subroutine proposed by Gudehus et al. (2008). (The coded models are available for free download from www.soilmodels.info).

The basic hypoplastic clay model presents a framework similar to that of any other critical state soil mechanics-based model. Figure 2 shows the bi-logarithmic compression law in the $\ln(1+e) \sim \ln(p'/p_r)$ plane. The isotropic normal compression line is described using the equation:

$$\ln(1+e) = N - \lambda^* \ln\left(\frac{p'}{p_r}\right) \tag{1}$$

where e is the void ratio, p' the mean effective stress and p_r = 1 kPa a reference stress. The parameters N and λ^* define its position and slope respectively. The parameter κ^* controls the slope of the isotropic unloading line in the same plane and the isotropic compression line of over-consolidated soil. The slope of the critical state line M is defined through the critical state friction angle φ_c:

$$M = \frac{6 \sin \varphi_c}{3 - \sin \varphi_c} \tag{2}$$

with identical meaning to other critical state soil mechanics-based models. To correctly represent the position of the critical state line, parameter O_c=1.5 controlling relative positions of isotropic normal compression line and critical state line has been included in the model;

for more details see Ragni et al. (2016). Finally, the description of the basic model is completed by the parameter υ, which controls the shear modulus and reads:

$$\upsilon = \frac{3r\left(\lambda^* + \kappa^*\right) - 4\kappa^*}{6r\left(\lambda^* + \kappa^*\right) + 4\kappa^*} \tag{3}$$

where r is the ratio of the bulk modulus in isotropic compression at the isotropic normally consolidated state and the shear modulus in undrained shear.

In order to model the effects of soil softening and remoulding due to plastic straining, the model was enhanced with the implementation of soil sensitivity, which required a sensitivity state variable s and three parameters k, A and s_f to be introduced (Mašín 2007). Sensitivity s is quantified by the ratio of intact and reconstituted soil shear strength, as defined in Cotecchia & Chandler (2000). s_f is the value of sensitivity in reconstituted conditions and can generally be assumed as unity The parameter k controls the rate of the sensitivity degradation:

$$\dot{s} = -\frac{k}{\lambda^*}\left(s_{ini} - s_f\right)\dot{\varepsilon}^d \tag{4}$$

where s_{ini} and s_f represent the initial and final values of sensitivity, and $\dot{\varepsilon}^d$ is the damage strain rate. The parameter A, which only has a minor effect on the results, controls the relative importance of the volumetric strain ε^v and shear strain ε^s components:

$$\dot{\varepsilon}^d = \sqrt{\left(\dot{\varepsilon}^v\right)^2 + \frac{A}{1 - A}\left(\dot{\varepsilon}^s\right)^2} \tag{5}$$

The equation for the normal compression line shown in Figure 2 can be then updated, accounting for sensitivity, as follows:

$$\ln(1+e) = N - \lambda^* \ln\left(\frac{p'}{p_r}\right) + \lambda^* \ln(s) \tag{6}$$

2.3 Soil description

The hypoplastic constitutive relation for structured clays was adopted for its suitability to investigate the effects of spudcan penetration and consolidation while allowing the characterisation of the resulting undrained *VHM* capacity. The choice of parameters describes a natural soil encountered in the Laminaria field, off the Northern Coast of Western Australia. This carbonate silty clay has a particle distribution of about 10% sand, 70% silt and 20% clay and a specific unit weight as a function of the depth w (in unit of m) of $\gamma' = 5.6 + 0.022\, w$ kN/m^3 (Randolph et al. 1998). Experimental investigation in a geotechnical centrifuge provided an undrained shear strength profile $s_u = 2.2\, w$ kPa using T-bar tests (Ragni et al. 2016). Previous studies by Erbrich (2005) and Amodio et al. (2015) on a similar soil highlighted a high degree of in-situ sensitivity, from 3.5 up to 20, due to its high content of calcium-carbonate and grain crushing at increasing stress level. Cyclic T-Bar episodes in a geotechnical centrifuge revealed a sensitivity s = 2.9; this is considerably lower than the values reported in Erbrich (2005), due to the continuing testing and remoulding of the silty clay used in the centrifuge.

A constant value of the over-consolidation ratio $OCR = 1.205$ was calculated from the model equations to initialise the void ratio in the soil for K_0 normally consolidated conditions. It should be noticed that, differently from traditional soil mechanics definition, in hypoplasticity a normally consolidated profile is characterised by $OCR > 1$, as OCR represents the ratio of Hvorslev equivalent pressure over mean effective stress p'. Jaky (1948) provided the earth pressure coefficient at rest $K_0 = 1\text{-}\sin\varphi_c = 0.441$.

Soil permeability k_w governs the excess pore pressure build-up in penetration and subsequent dissipation rate during the consolidation stage. Following basic laboratory tests, described in Mahmoodzadeh et al. (2015) and Ragni et al. (2106), an isotropic permeability was assigned to the soil as follows:

$$k_w = \gamma_w m_v c_v = \frac{\gamma_w c_v \lambda^*}{\sigma_v'} \tag{7}$$

where γ_w is the unit weight of water, c_v the coefficient of consolidation and σ_v' the vertical effective stress. Due to the bi-logarithmic nature of the compressive law illustrated in Figure 2, the coefficient of compressibility is calculated as $m_v = \lambda^*/ \sigma_v'$. The coefficient of consolidation c_v measured via the oedometer test was:

$$c_v = \frac{\sigma_v'}{10 + 0.478\ \sigma_v'} \tag{8}$$

The units of c_v and σ_v' are m^2/year and kPa, respectively.

The parameters related to the basic model and sensitivity are listed in Table 1. These match the values adopted in Ragni et al. (2016), where the same carbonate silty clay was investigated, with the implementation of the same numerical model. The parameter calibration is described in Ragni et al. (2016), where basic laboratory tests (triaxial and oedometer tests) and retrospective simulations of boundary value problems (spudcan vertical penetration in geotechnical centrifuge) underpinned the procedure. All the necessary steps towards an accurate model calibration were taken in Ragni et al. (2016): for this reason, the model was also assumed to be suitable for the description of the problem here investigated.

2.4 From two-dimensional to three-dimensional analyses

The entire process of spudcan penetration with a phase of consolidation, followed by excursions of combined displacements, is a difficult problem to model numerically. Due to the mono-directional geometry of the problem, the penetration and consolidation were analysed in an axisymmetric model, without the need to recur to a three-dimensional model which would affect the efficiency of the analyses. LDFE model with coupled pore fluid-stress response allowed large strains generated during installation to be modelled and excess pore pressure variations to be captured. Moreover, the implementation of soil sensitivity contributed to the description of the installation effects. Eight-node elements with biquadratic displacement, bilinear pore pressure and reduced integration (termed CAX8RP in Dassault Systèmes 2012) were used to discretise the soil. However, simulation of multi-directional *VHM* problems required to move from the axisymmetric to a three-dimensional model. Due to the geometry of the problem under consideration, only half of the three-dimensional model (i.e. 180°), rather than a full 360° domain, needed to be considered. Twenty-node elements, with triquadratic displacement, trilinear pore pressure and reduced integration (C3D20RP in Dassault Systèmes 2012) allowed the simulation of coupled analyses and were used to discretise the soil.

The spudcan geometry is shown in Figure 3. It was modelled as a rigid body, given its much higher stiffness compared to the soil. The load-displacement response of the spudcan is represented by three degrees of freedom (vertical, horizontal and rotational) referring to the Reference Point (RP) and with the sign convention illustrated in Figure 3.

The three-dimensional soil domain was chosen as 3*D* vertically and 6*D* horizontally (see Figure 4), in order to minimise boundary effects and computational cost. This is a 'regular' domain size for undrained bearing capacity analyses using small-strain finite element method.

In contrast, the soil extensions were as large as 20*D* in the axisymmetric LDFE analyses of penetration and consolidation, to avoid any potential boundary effect. Three-dimensional analyses involving a larger soil domain (20*D* vertically and 40*D* horizontally) offered a solution extremely close to the smaller domain (an average of -1.6% in the loading response), while at the same time dramatically increasing the computational cost by ~400%. Since the aim of the paper was to isolate the bearing capacity offered by the footing alone, the jack-up leg connected to the spudcan was not modelled intentionally in the three-dimensional analyses (RHS of Figure 5a, b, c), whereas it was involved in the LDFE study to capture the effects of the installation process properly (LHS of Figure 5a, b, c).

After creating the three-dimensional geometry by revolving the axisymmetric model around a 180° angle, particular attention was dedicated to the mapping strategy. Once the spudcan was penetrated to the target depth with LDFE analyses, the resulting effective stresses and material properties were mapped to the integration points of the three-dimensional model, whereas the excess pore pressures were mapped to the nodes. The mapping strategy was such that every integration point and node of the three-dimensional model was searched in the axisymmetric model, by conversion of its three-dimensional coordinates to the axisymmetric corresponding counterpart. Then, each field variable was interpolated within the eight-node axisymmetric element which contains the integration point or the node. A mesh density similar to that of the axisymmetric model is desirable to minimise the error in interpolation. For the limited volume of soil replacing the leg which was present in LDFE analyses, it was assumed that the field variables were equal to those at the nearest integration point or node. Figure 5 shows an example of the results obtained when mapping a) excess pore pressures, b) sensitivity and c) void ratio from the LDFE analyses (LHS) in the 3D model (RHS). The minimal discrepancy between the vertical force applied to the spudcan in the two-

dimensional and three-dimensional model after mapping (limited to 4%) confirmed the validity of the mapping procedure.

2.5 Definition of the yield surface

In order to interpret the results, an equation to describe the shape of the yield surface in the *VHM* space must be first defined. It is here outlined in the form proposed by Martin & Houlsby (2000) for heavily overconsolidated clay and later expanded by Vlahos et al. (2008) to account for tensile capacity. It reads:

$$f = \left(\frac{H}{h_0 V_0}\right)^2 + \left(\frac{M/D}{m_0 V_0}\right)^2 - \frac{2 e_s HM/D}{h_0 m_0 V_0^2} - \left(\frac{4}{(1+\chi)^2}\right)\left(\frac{V}{V_0}+\chi\right)^2\left(1-\frac{V}{V_0}\right)^2 = 0 \quad (9)$$

where h_0 is the peak of horizontal over vertical capacity in the *VH* (M=0) plane, m_0 is the peak of moment over vertical capacity in the *VM* (H=0) plane, e_s represents the eccentricity of the surface in *HM* plane, V_0 is the vertical bearing capacity and χ is the ratio of peak tensile over compressive capacity.

If a non-vertical force term Q is defined as:

$$Q^2 = \left(\frac{H}{h_0}\right)^2 + \left(\frac{M/D}{m_0}\right)^2 - \frac{2 e_s HM/D}{h_0 m_0} \quad (10)$$

then Equation 9 can be simplified and re-written as:

$$f = \left(\frac{Q}{V_0}\right)^2 - \left(\frac{4}{(1+\chi)^2}\right)\left(\frac{V}{V_0}+\chi\right)^2\left(1-\frac{V}{V_0}\right)^2 = 0 \quad (11)$$

and the results presented in the non-dimensional Q/V_0-V/V_0 plane. The advantage of such simplification is that, provided the optimal set of parameters, all the tests should lay on the same curve. Zhang et al. (2014a) showed Equation 9 to be applicable also for spudcans experimentally penetrated into soft normally consolidated kaolin clay, with recommended parameters values at a penetration depth w/D = 1.0 included in Table 2.

2.6 *VHM* investigation strategy: three-dimensional analyses

Investigation of the undrained *VHM* capacity of a spudcan following penetration and consolidation in silty clay is the main focus of this paper. For numerical stability and computational efficiency, the spudcan-soil interaction was simplified with a tie constraint, which tends to overestimate the capacity. However, further analyses involving frictionless contact showed a marginal effect (2.5% difference in pure rotation) on the magnitude of the combined bearing capacity.

Roughly 15000 elements were used to discretise the soil domain. The minimum element size around the spudcan was 0.045 D; further simulations reducing this value to 0.02 D proved to have a marginal effect of 1% while, at the same time, increasing the computational effort by 700%. Further reduction of the element size in relation to the spudcan displacements is thought to generate excessive mesh distortion (Yi et al. 2014) and cause analysis instability.

After penetrating the spudcan to a target depth w, allowing for a period of consolidation under constant vertical load and mapping the state variables to the three-dimensional model, probe and swipe tests were carried out in order to investigate the combined bearing capacity of the spudcan. In case of probe tests (Tan 1990, Gottardi et al. 1999), either a horizontal displacement of the spudcan u, or a rotation θ was applied at a constant value of V, which was assumed as a fraction of the vertical bearing capacity. These tests were used to investigate the underlying failure mechanisms and the effect of different excess pore pressure distributions.

In the swipe tests, firstly proposed by Tan (1990), a horizontal displacement u, a rotation θ, or a combination of both was applied, while the spudcan depth w was held constant, so as to generate load paths where V gradually reduced as the response in H and M increased. Provided a sufficiently high ratio of elastic over plastic stiffness of the soil (Tan 1990, Martin 1994, Martin & Houlsby 2000), such load paths are thought to closely track the yield surface. All the swipe tests started from the same V (with $H = M = 0$) and moved along different paths of the three-dimensional surface, according to the u:$D\theta$ ratio, so to determine the capacity surface in the VH and VM planes. Swipe tests were preferred to probe tests to describe the yield surface, for the latter start within the surface and would not offer a straightforward identification of the yielding point, due to accumulation of plastic deformations from the very onset of the test (as real soil does not have the perfect elastic–plastic yield surface boundary we attempt to model it by). When the HM response of each swipe was plotted at constant V values (i.e. sectioning the yield surface parallel to the H-M plane at regular intervals along the V axis), the surface eccentricity was observed, which ultimately offered a comprehensive picture of the yield surface in the VHM space.

3. RESULTS

3.1 Vertical installation and consolidation

Results from the parametric study presented in Ragni et al. (2016) in terms of increasing bearing pressure q with depth are shown in Figure 6. The dashed line represents the load-penetration curve of a continuous spudcan penetration with no stoppage. Figure 6a and b respectively show how penetration is affected by different lengths of consolidation and vertical loads held during the pause, at increasing consolidation depths w/D = 1.0; 1.5; 2.0. In particular, increasing dimensionless consolidation time $T = c_v t/D^2$ (varying from 0.001 to 0.5, where t is the dimensional time) is demonstrated to generate a higher peak in bearing capacity q upon further penetration. A reduction of the load (i.e. the pressure) held in consolidation

q_{cons} = 1.0; 0.75; 0.5 q_{ref} (where q_{ref} is the pressure achieved in continuous penetration) leads to the opposite effect. These data simulated the installation effects and represented the starting point of the following *VHM* investigation.

The results presented in the next section compare the combined bearing capacities of a spudcan installed to w/D = 1, followed by a period of consolidation T = 0; 0.01; 0.05 and where the load held during the pause was q_{cons} = 1.0 q_{ref} (tests reported in black in Figure 6a).

3.2 *Example load paths:* capacity increase under pure translation or rotation

It is common practise in jack-up installation to increase the vertical load by pumping sea-water into specifically designed ballast tanks to facilitate the spudcan penetration. This vertical load is then reduced during operational conditions once the installation is completed and ballast tanks emptied. The combined capacity of the footing (i.e. the size of the yield surface) can be considered as a function of the vertical capacity V_0 (with T = 0) achieved during installation, as schematically illustrated in Figure 7. However, if this load is held for a certain amount of time t, an increase in vertical capacity is observed due to consolidation, leading to a higher $V_0^* = V_0(T)$. As a result, also the combined capacity will increase accordingly.

The probe tests presented in Figures 8 and 9 investigated the response to pure horizontal displacement u and pure rotation θ of a spudcan installed to a depth w/D = 1.0 and were simulated at a model scale, at enhanced gravity of 200g and D = 60 mm. A reference case without consolidation was compared against two cases involving increasing consolidation T = 0.01; 0.05. In order to simulate real case scenarios, the tests were carried out by reducing V to 0.5; 0.75; and 0.9 of the value achieved in installation (and held for consolidation, when this was included), labelled as V_0 (T = 0) in Figure 7.

All results are presented in a dimensionless fashion, unless differently stated. When normalising H and M, the adopted ultimate vertical capacity V_0^* refers to the expanded yield surface for the cases involving consolidation, i.e. V_0 (T = 0.01) and V_0 (T = 0.05) in Figure 7. Such V_0^* values were obtained from Figure 6a, where the recorded peak in the load-penetration curves after consolidation at w/D = 1 revealed an increase of the original bearing capacity V_0 = 665.0 N equal to 23% for T = 0.01 (V_0^* = 818.1 N) and 37% for T = 0.05 (V_0^* = 914.4 N). As shown in Figure 5, a period of consolidation causes a certain amount of settlement of the footing, which increases with increasing T and q_{cons}. Consequently, it should be noticed that when referring to an increase in combined bearing capacity, such an improvement should be regarded as a combination of the effect of consolidation itself and increased depth w/D due to settlement, which is also responsible for an increase in capacity (Zhang et al. 2011, Wang & Bienen 2016).

In the tests reported in Figure 8, a final horizontal displacement u/D = 0.03 was targeted (please note that some of the tests failed to converge before reaching the final displacement), while rotation θ was not allowed. Similarly, Figure 9 involved a rotation θ = 4°, while no horizontal displacement was allowed. Regardless of the fraction of vertical load at which the tests were carried out (V is 0.5; 0.75 or 0.9 times V_0 (T = 0)), a higher initial stiffness is observed for increasing T, which degrades at increasing strain levels.

As summarised in Table 3, longer periods of consolidation result in larger increases in H and M capacity, as expected and already observed for the V capacity. Towards the capacity surface apex, i.e. with V approaching V_0, the HM cross-section becomes smaller (see Figures 1 and 7), such that the H and M capacity is lower even for long periods of consolidation (Figures 8 and 9).

The next sections explore the reasons behind the increase in combined capacity observed in Figures 8 and 9, highlighting differences in failure mechanism and excess pore pressure distribution caused by consolidation.

3.2.1. Failure mechanism

Figures 10 and 11 show the resultant displacement contour plots observed in the *uw* plane, with an applied vertical load $V = 0.5\ V_0$ ($T = 0$), following $u/D = 0.03$ and $\theta = 4$ respectively (load-displacement curves in Figures 8a and 9a), for a) the case with no consolidation and b) a consolidation period $T = 0.05$.

When observing Figure 10 ($u/D = 0.03$), similarities can be found with the study presented by Zhang et al. (2011) (see Figure 10 inset) on kaolin clay, with a prevalent sliding mechanism at the base and scoop mechanism above the spudcan. The position of the centre of the scoop mechanism is also similar for the depth $w/D = 1.0$ analysed. A shallow mechanism can be observed in both cases, which extends to the soil surface as in Zhang et al. (2011). Differences with Zhang et al. (2011) lie in the increased asymmetry of the failure mechanisms presented here. The test described is such that passive and active zones are activated as a result of the footing moving horizontally. Consequently, the adoption of an advanced constitutive model can better describe the different stiffness in loading and unloading, as well as the different strength in compression and extension. On the other side, the adoption of a simpler constitutive model adopted in Zhang et al. (2011) (Tresca model and total stress analyses) can be responsible for an incorrect symmetry. The higher heterogeneity in the silty clay due to higher shear strength (2.1 kPa/m compared with 1.2 kPa/m in kaolin) may also be responsible for the increased asymmetry. Also, when the footing is idealised as wished-in-place (Templeton et al. 2005, Templeton 2009, Zhang et al. 2011), the presence of a soil cavity above the spudcan is denied. While the general shape of

the failure mechanism is similar for cases with and without a consolidation period, consolidation is shown to increase the size (Figure 9).

Similar conclusions can be drawn from Figure 11 ($\theta = 4°$), with the enlarged failure mechanism of comparable shape. As already observed in Zhang et al. (2011) (Figure 11 inset), the mechanism is rotational, with centre of rotation close to the RP at $w/D = 1$. Differently from Zhang et al. (2011) though, in this case the failure mechanism extends to the soil surface, as a consequence of the correct modelling of the installation procedure and the improved constitutive model implemented.

It is clear that although the failure mechanisms presented in Figures 10b and 11b ($T = 0.05$) are slightly more extended than their counterpart without consolidation, this mobilisation of larger portions of soil is not sufficient on its own to justify the increase in combined capacity observed in Figures 8 and 9. For this reason, the next section investigates the influence of dissipation of excess pore pressures on the foundation capacity under combined loading.

3.2.2. Excess pore pressure distribution

The penetration process causes the generation of excess pore pressures in the region of soil around the spudcan, due to the permeability properties of the soil. However, with a load-hold period following the penetration, dissipation of excess pore pressures is observed. Bienen et al. (2015) experimentally showed that holding the full vertical load mobilised at $w/D = 1.0$ for a period of time as long as $T = 0.05$, the excess pore pressure ratio $B_q = \Delta u/q_{nom}$ (being Δu the excess pore pressures at the base of the spudcan and q_{nom} the bearing pressure during consolidation) reduces about 40% from the value recorded before consolidation. As a consequence, the void ratio will also reduce, as shown in Figure 12, where the void ratio distribution for the case without consolidation (LHS) and with consolidation $T = 0.05$ (RHS) are compared. The reduction in void ratio is accompanied with the increase in the undrained

shear strength s_u. The enhancement of undrained strengths ultimately affects the combined capacity of the footing, as observed in the increased responses given by the numerical scenarios involving consolidation in Figures 8 and 9.

The assumption of undrained conditions can be formulated during the *VHM* investigation. Figures 13 and 14 confirm the behaviour described above by showing the distribution of excess pore pressures Δu (kPa) when $u/D = 0.03$ and $\theta = 4^o$ are applied a) immediately after penetration or b) after a consolidation period $T = 0.05$. Figures 13a and 14a show higher levels of Δu developing due to the elevated excess pore pressures sustained from the spudcan penetration process. In contrast, Figures 13b and 14b show much lower Δu as a result of the dissipation during the consolidation stage. Regions with negative Δu are also observed below the base of the footing, generated when u or θ are applied starting from $\Delta u \sim 0$. The negative excess pore pressure contributes to the generation of suction, causing increase in capacity.

3.3 Quantification of yield surface expansion due to consolidation

3.3.1. Size and shape along the vertical load axis

Figure 15 reports the results of the numerical SSFE simulations of swipe tests by plotting the load paths in terms of Q/V_0 - V/V_0 for scenarios a) with no consolidation ($T = 0$) and with consolidation of b) $T = 0.01$ and c) $T = 0.05$. All the results were normalised by the respective increased bearing capacity V_0^*, which was also the starting point of the test (see inset Figure 15). In order to offer a straightforward comparison with available centrifuge experimental data later presented, the tests were simulated at a model scale, at enhanced gravity of 100g (swipe tests carried out are summarised in Table 4). Numerical simulations of the penetration-consolidation-penetration were necessary to determine the increased V_0^*. Increments of 32% and 69% against V_0 ($T = 0$) = 305.6 N were obtained for $T = 0.01$ ($V_0^* = 403.6$ N) and $T = 0.05$ ($V_0^* = 518.8$ N), respectively.

For each consolidation time, an equation of the yield surface (black curve) was determined to best fit the experimental results, according to Equation 11. The fitting exercise concentrated on the optimisation of h_0, m_0 and e_s through least squares regression. Centrifuge data of spudcan penetration followed by immediate extraction provided a ratio of tensile to compressive vertical capacity of $\chi = 0.5$. The same value was adopted for the cases involving consolidation, for no sufficient experimental data were available to determine an exact value. The value $\chi = 0.5$ is slightly lower than presented in Zhang et al. (2014a) for soft clay ($\chi = 0.6$), possibly due to the higher sensitivity of the silty clay ($s = 2.9$ for silty clay and 2.2 for soft clay), which causes the remoulded soil above the spudcan to offer a lower resistance in extraction.

The fitting exercise returned $h_0 = 0.297$ and $m_0 = 0.147$ for $T = 0$, offering the good agreement shown in Figure 14a. As a period of consolidation was taken into account, h_0 were observed to increase to 0.309 (+4.0%) and 0.387 (+30.3%) (Figure 14b and c), whereas m_0 presented only a marginal increase to 0.151 (+2.7%) for $T = 0.01$and 0.152 (+3.4%) for $T = 0.05$. Interestingly, not only is the absolute response in terms of H and M enhanced after consolidation, but also the normalised response increases in terms of h_0 and m_0. This means that consolidation does not simply scale up the size of the yield surface, with ratios of vertical over combined capacities unchanged, but also modifies its shape, in line with the observations of Figures 10 and 11 in terms of different sizes of the failure mechanism.

Zhang et al. (2014b) adopted a slightly different equation to describe the yield surface in the *VHM* space. Nonetheless, the parameters h_0 and m_0 only determine the size of the yield surface and can thereby be compared with the present study. Numerical simulations for soft clay in Zhang et al. (2014b) resulted in lower values of $h_0 = 0.224$ and $m_0 = 0.120$ for the same embedment depth $w/D = 1$, $T = 0$ and a sensitivity increased to $s = 3$ (close to $s = 2.9$ for silty clay). The reasons for the difference with the silty clay values can be found in the lower

shear strength profile (1.2 kPa/m compared with 2.1 kPa/m) and slightly higher sensitivity assumed (3 compared with 2.9), which would result in a lower *HM* response. The increasing consolidation period generates an effect similar to the increasing embedment depth observed in Zhang et al. (2014). In particular, a significant increase with the embedment depth of spudcan is observed for h_0 (+39% from w/D = 1 to w/D = 3), whereas a lower increase is observed for m_0 (+13% from w/D = 1 to w/D = 3).

3.3.2. Size and shape in planes of constant vertical load

The least square regression introduced above determined a constant eccentricity e_s = 0.1 for T = 0; 0.01; 0.05. The complete set of parameters (h_0, m_0, e_s, χ) was used to plot sections of the yield surfaces in the normalised plane H/V_0-M/DV_0, at constant vertical load V of 0.5; 0.75 or 0.9 times V_0 (or V_0^*), for increasing T = 0; 0.01; 0.05, as illustrated in Figure 16. Accordingly to the rugby ball-shaped yield surface schematically outlined in Figure 7, a reduction in *HM* capacity is observed for increasing V (from red to green), since the loading state is moved incrementally closer to the ultimate vertical capacity V_0 (or V_0^*). Having assumed the swipe tests to move along the yield surface, the intercepted response of each swipe test at the corresponding V/V_0 was also plotted as a dot in the same plane, to illustrate the parameter fit obtained through least squares regression.

The increase in h_0 due to consolidation is reflected in Figure 16, with the yield surface widening along the H/V_0 axis as the consolidation period increases. In contrast, the intercept on the M/DV_0 axis (i.e. H/V_0 = 0) is almost unchanged, reflecting the minimal increase in m_0 due to consolidation. As a consequence, an increasingly different shape of the yield surface section is observed as consolidation time increases.

On the other hand, the distribution of load path intercepts at constant V/V_0 ratios shows how the eccentricity is not affected by a period of consolidation, as a constant value $e_s \sim 0.1$ fits the results throughout.

3.4 Supportive evidence from centrifuge testing

A series of experimental swipe tests was carried out on carbonate silty clay in the geotechnical beam centrifuge at the University of Western Australia at enhanced gravity level of 100g. The sample was prepared mixing the soil with minimum amount of added water and consolidated in flight for five days to achieve normally consolidated conditions. T-bar tests measured an average shear strength profile of 1.14 kPa/m prior to the spudcan tests and 2.01 kPa/m immediately after. The spudcan tests lasted approximately three days. The spudcan diameter was D = 60 mm with geometry as illustrated in Figure 3 and it was equipped with five pressure transducers, in order to monitor excess pore pressure variations throughout the test. Only a limited number of previous studies modelled the lattice leg above the spudcan (Springman & Schofield 1998, Li et al. 2012, 2014, Yang et al. 2014); in this case a cylindrical aluminium shield protected the leg equipped with axial and bending strain gauges. A soft silicon sealant was used to seal the gap between the shield and the spudcan; this ensured minimal load transfer between the two, allowing in this way to record only the loading acting on the spudcan. A detailed description of the apparatus can be found in Zhang et al. (2013, 2014a).

In the experiments, the footing was first penetrated to the target depth w/D = 1.0 at a rate of v = 0.2 mm/s, with the normalised velocity $V = vD/c_v > 100$ to guarantee undrained conditions (Finnie 1993, Chung et al. 2006, Cassidy 2012). Then, a reference set of four tests involved displacement and/or rotation immediately after vertical penetration to w/D = 1.0, whereas in the remaining seven tests, a period of consolidation (either T = 0.01 or 0.05) was

allowed between the end of the penetration and the swipe test. All u:$D\theta$ paths were applied at a rate such that undrained conditions were guaranteed. Table 4 summarises all the swipe tests carried out.

Figure 17 reports the load paths in terms of Q/V_0-V/V_0: all the tests started from V_0 reached prior to consolidation (see inset Figure 17), as the increased V_0^* was unknown prior to the swipe tests. The V_0^*/V_0 ratios determined numerically were adopted to normalise the experimental results.

In the same way as the numerical case, a constant values of $\chi = 0.5$ was used. A constant $e_s = 0.1$ was also assumed from the numerical results, for the experimental tests only covered part of the yield surface in the H/V_0-M/DV_0 plane and thus could not offer a precise estimation of the eccentricity.

The parameters h_0 and m_0 estimated through least square regression appear to be consistently lower than the numerical counterparts (Table 1) as well as the values presented in Zhang et al. (2014a) for soft clay. This can be attributed to a consolidation process of the silty clay sample only partially completed in the centrifuge, as demonstrated by the increase over time of the shear strength profiles from T-bar tests. Fully consolidated conditions are only achieved by spinning the sample for a long time; for this reason the dedicated five days of consolidation may not have been sufficient. When modelling the sample numerically, a fully consolidated profile is automatically achieved. This leads to a shear strength profile (2.1 kPa/m) higher than the experimental case and potentially to the discrepancy in the results. Also, the experimental loading paths involving consolidation initially lie inside the expanded yield surface, as it was not possible to experimentally determine V_0^* a priori. This leads to uncertainties on when they rejoin and begin to track the yield surface, noting that the concept of pure elastic-plastic response of soil in a macro element model is just a numerical

approximation. On the other hand, although it represents a reasonable assumption, the hypoplastic model may not strictly track the yield surface during the vertical unloading observed during swipe tests (see Mašín and Herle 2007).

Nonetheless, a similar qualitative trend was captured in terms of h_0 and m_0 increase with T. In particular, the original $h_0 = 0.186$ for $T = 0$ increased significantly to $h_0 = 0.215$ (+15.6%) for $T = 0.01$ and $h_0 = 0.268$ (+44.1%) for $T = 0.05$; whereas $m_0 = 0.075$ for $T = 0$ showed a more moderate increase to $m_0 = 0.085$ (+13.3%) for $T = 0.01$ and $m_0 = 0.089$ (+18.6%) for $T = 0.05$. Table 2 offers an overview of the increases in h_0 and m_0 with T for both the numerical and the experimental cases.

The following section provides a comparison with the state-of-the-art procedure to estimate the combined capacity offered in the current international guidelines for jack-ups (ISO 2012), before the outcomes of the paper are summarised in the final section.

4. RECOMMENDATIONS FOR ISO (2012) GUIDELINES

In the current guidelines offered in ISO (2012):

1. the ultimate vertical bearing capacity V_0 is established according to the vertical preload;
2. only further penetration can generate an increase in V_0;
3. spudcan geometry and soil properties at the installation depth determine the maximum horizontal and moment capacity, which define the size of the yield surface;
4. guidance is only offered for clayey and sandy soils, not for silty material.

With regard to points 1) and 2), Figure 6 demonstrated that V_0 is indeed established according to the depth reached in installation, but also that it can be substantially modified due to the installation process, remoulding and through consolidation. As

described in point 3), ISO (2012) does not take into account the effects of consolidation in the determination of combined capacity, as this is determined as a function of the installation depth. This paper demonstrated the effect of consolidation on the vertical and, consequently, the combined capacity. Such findings are important as they reveal the potential to achieve the targeted capacity at a shallower embedment through a planned consolidation period, should the leg length be a limiting factor in installation. Future research will establish the reliability of the enhanced capacity under cyclic loading from metocean actions. The findings can also guide probabilistic considerations on the reduced failure probability (i.e. capacity to withstand storm events with increasingly higher return period) as a function of the degree of consolidation achieved under the vertical load held over time. Finally, ISO (2012) does not offer any guidance in terms of assessment of the *VHM* capacity for spudcan installed in silty clay. In this sense, the paper offers insights aimed at easing the difficult and challenging installation process in these soils.

5. CONCLUDING REMARKS

A numerical investigation of the influence of consolidation on spudcan combined capacity in silty soil was presented. An increased combined capacity in terms of *H* and *M* was shown in the tests where a period of consolidation followed the initial vertical penetration. In particular:

- The results demonstrated the importance of simulating the entire process of spudcan installation and potential consolidation stage before a *VHM* investigation is carried out. Similar conclusions were drawn in Zhang et al. (2014a,b) for spudcans penetrated into soft clay. On the other hand, a load-hold period is demonstrated to dramatically affect the excess pore pressure distribution, as not only does it have an influence on the vertical (Ragni et al. 2016) but also on the combined capacity (Figures 8 and 9). It

is thus important to treat the problem as a whole, rather than as a sequence of independent stages from installation to operation. Since the present study is limited to one embedment $w/D = 1$, future research shall take into account the effect of different installation depths, as it is demonstrated in Zhang et al. (2014a,b) to have an influence on the size and shape of the yield surface;

- The adoption of an advanced constitutive model revealed asymmetric failure mechanisms related to pure translation or rotation, in contrast to the results generated by the assumption of simple constitutive models, such as Tresca, where symmetric failure mechanisms can be incorrectly predicted;
- Not only does consolidation lead to an enhanced absolute response in terms of H and M, but also to increased values of h_0 and m_0. As these relate the size of the surface to the (increased) uniaxial vertical capacity, increases in h_0 and m_0 signal a disproportionally larger increase in horizontal and moment capacity.

ACKNOWLEDGEMENTS

This work forms part of the activities of the Centre for Offshore Foundation Systems (COFS), which is currently supported as one of the primary nodes of the Australian Research Council (ARC) Centre of Excellence for Geotechnical Science and Engineering (CE110001009) and as a Centre of Excellence by the Lloyd's Register Foundation. Lloyd's Register Foundation helps to protect life and property by supporting engineering-related education, public engagement and the application of research. The second and fifth authors are the recipients of ARC Postdoctoral (DP110101603) and Laureate Fellowships (FL130100059), respectively. The authors are grateful for these supports.

REFERENCES

Amodio, A., Chang, T.M., Kong, V. and Erbrich C.T. (2015). The effects of jack-up installation procedures on spudcan capacity in offshore carbonate sediments. *Proc. 3rd International Symposium on Frontiers in Offshore Geotechnics (ISFOG), Oslo, Norway, Vol. 2, pp. 1253-1260.*

Bienen, B., Byrne, B.W., Houlsby, G.T., & Cassidy, M.J. (2006). Investigating six-degree-of-freedom loading of shallow foundations on sand. *Géotechnique, Vol.56, No. 6, pp. 367-380.*

Bienen, B. and Cassidy, M.J. (2013). Set up and resulting punch-through risk of jack-up spudcans during installation. *Journal of Geotechnical and Geoenvironmental Engineering, Vol. 139, No. 12, pp. 2048-2059.*

Bienen, B., Ragni, R., Cassidy, M.J. and Stanier, S.A. (2015*).* Effects of consolidation under a penetrating footing in carbonate silty clay. *Journal of Geotechnical and Geoenvironmental Engineering, Vol. 141, No. 9, 04015040.*

Bransby, M.F. and Randolph, M.F. (1998). The effect of skirted foundation shape on response to combined V-MH loadings. *Proc. 8th International Offshore and Polar Engineering Conference, Montreal, Canada.*

Butterfield, R. and Ticof, J. (1979). Design parameters for granular soils (discussion contribution). *Proc. 7th ECSMFE, Brighton, UK, Vol. 4, pp. 259-261.*

Cassidy, M.J. and Houlsby, G.T. (1999). On the modelling of foundations for jack-up units on sand. *Proc. Offshore Technology Conference, Houston, Texas.*

Cassidy, M.J. (2012). Experimental observations of the penetration of spudcan footings in silt. *Géotechnique, Vol. 62, No. 8, pp. 727-732.*

Chung, S.F., Randolph, M.F. and Schneider, J.A. (2006). Effect of penetration rate on penetrometer resistance in clay. *Journal of geotechnical and geoenvironmental engineering, Vol. 132, No. 9, pp. 1188-1196.*

Cotecchia, F. and Chandler R.J. (2000). A general framework for the mechanical behaviour of clays. *Géotechnique, Vol. 50, No. 4, pp. 431-447.*

Dean, E.T.R., James, R.G., Schofield, A.N. and Tsukamoto, Y. (1997). Theoretical

modelling of spudcan behaviour under combined load. *Soils and Foundations, Vol. 37, No. 2, pp. 1-15.*

Dassault Systèmes. (2012). Abaqus 6.12 User's manual.

Erbrich, C.T. (2005). Australian frontiers–spudcans on the edge. *Proc. 1st International Symposium on Frontiers in Offshore Geotechnics (ISFOG), Perth, Australia, Vol. 1, pp. 49-74.*

Finnie, I.M.S. (1993). Performance of shallow foundations in calcareous soil. *PhD Thesis. University of Western Australia, Perth, Australia.*

Gottardi, G., Houlsby, G.T. and Butterfield, R. (1999). Plastic response of circular footings on sand under general planar loading. *Géotechnique, Vol. 49, No. 4, pp. 453-470.*

Gourvenec, S. (2007). Shape effects on the capacity of rectangular footings under general loading. *Géotechnique, Vol. 57, No. 8, pp. 637-646.*

Gudehus, G., Amorosi, A., Gens, A., Herle, I., Kolymbas, D., Mašín, D., Muir Wood, D., Nova, R., Niemunis, A., Pastor, M., Tamagnini, C. and Viggiani, G. (2008). The soilmodels.info project. *International Journal for Numerical and Analytical Methods in Geomechanics, Vol. 32, No. 12, pp. 1571-1572.*

Hossain, M.S., Hu, Y., Randolph, M.F. and White, D.J. (2005). Limiting cavity depth for spudcan foundations penetrating clay. *Géotechnique, Vol. 55, No. 9, pp. 679-690.*

Houlsby, G.T. and Puzrin, A.M. (1999). The bearing capacity of a strip footing on clay under combined loading. *Proc. of the Royal Society of London A: Mathematical, Physical and Engineering Sciences, Vol. 455, No. 1983, pp. 893-916.*

Hu, Y. and Randolph, M.F. (1998). A practical numerical approach for large deformation problems in soil. *International Journal of Numerical and Analytical Methods in Geomechanics, Vol. 22, No. 5, pp. 327-350.*

Hu, P., Wang, D., Stanier, S.A. and Cassidy, M.J. (2015). Assessing the punch-through hazard of a spudcan on sand overlying clay. *Geotechnique, Vol. 65, No. 11, pp. 883-896.*

International Organization for Standardization (ISO) (2012) - Petroleum and natural gas industries - Site-specific assessment of mobile offshore unit - Part 1: Jack-ups. *Geneva, Switzerland.*

Jacky, J. (1948). Pressure in soils. *Proc. of the 2nd International Conference on Soil Mechanics and FoundationEngineering. London, UK, pp. 103-107.*

Li, Y.P., Lee, F.H., Goh, S.H., Yi, J.T. and Zhang, X.Y. (2012). Centrifuge study of the effects of lattice leg on penetration resistance and bearing behavior of spudcan foundations in NC clay. *Proc. 31st International Conference on Offshore Mechanics and Arctic Engineering (OMAE), Rio de Janeiro, Brasil, pp. 79-86.*

Li, Y.P., Zhang, X.Y., Lee, F.H., Goh, S.H., Wu, J.F. and Yi, J.T. (2014). Effect of lattice leg on penetration resistance of spudcan foundations-Physical and numerical modeling. *Proc. 8th International Conference on Physical Modelling in Geotechnics (ICPMG), Perth, Australia, pp. 515-521.*

Mahmoodzadeh, H., Wang, D. and Randolph, M.F. (2015). Interpretation of piezoball dissipation testing in clay. *Geotechnique, Vol. 65, No. 10, pp. 831-842.*

Martin, C.M. (1994) Physical and numerical modelling of offshore foundations under combined loads. *PhD Thesis. University of Oxford, UK.*

Martin, C.M. and Houlsby, G.T. (2000). Combined loading of spudcan foundations on clay: laboratory tests. *Géotechnique, Vol. 50, No. 4, pp. 325-338.*

Martin, C.M. and Houlsby, G.T. (2001). Combined loading of spudcan foundations on clay: numerical modelling. *Géotechnique, Vol. 51, No. 8, pp. 687-700.*

Mašín, D. (2007). A hypoplastic constitutive model for clays with meta-stable structure. *Canadian Geotechnical Journal, Vol. 44, No. 3, pp. 363-375.*

Mašín, D. and Herle, I. (2007). Improvement of a hypoplastic model to predict clay behaviour under undrained conditions. *Acta Geotechnica, Vol. 2, No. 4, pp. 261-268.*

Mašín, D. (2014). Clay hypoplasticity model including stiffness anisotropy. *Géotechnique, Vol. 64, No. 3, pp. 232-238.*

Nova, R. and Montrasio, L. (1991). Settlements of shallow foundations on sand. *Géotechnique, Vol. 41, No.2, pp. 243-256.*

Ragni, R., Wang, D., Mašín, D., Bienen, B., Cassidy, M.J. and Stanier, S.A. (2016). Numerical modelling of the effects of consolidation on the jack-up spudcan penetration. *Computers and Geotechnics, Vol. 78, pp. 25-37.*

Randolph, M.F., Hefer, P.A., Geise, J.M. and Watson, P.G. (1998). Improved seabed strength profiling using T-bar penetrometer. *Proc International Conference on Offshore Site Investigation and Foundation Behaviour - "New Frontiers", Society for Underwater Technology, London, UK, pp. 221-235.*

Roscoe, K.H. and Schofield, A.N. (1956). The stability of short pier foundations in sand. *British Welding Journal, Vol. 3, No. 8, pp. 343-354.*

Salciarini, D. and Tamagnini, C. (2009). A hypoplastic macroelement model for shallow foundations under monotonic and cyclic loads. *Acta Geotechnica, Vol. 4, No. 3, pp. 163-176.*

Schotman, G.J.M. (1989). The effects of displacements on the stability of jackup spudcan foundations. *Proc. Offshore Technology Conference, Houston, Texas, OTC 6026.*

Springman, S.M. and Schofield, A.N. (1998). Monotonic lateral load transfer from a jack-up platform lattice leg to a soft clay deposit. *Proc. Conference Centrifuge, Tokyo, Japan, pp. 563-568.*

Stanier, S.A., Ragni, R., Bienen, B. and Cassidy, M.J. (2014). Observing the effects of sustained loading on spudcan footings in clay. *Géotechnique, Vol. 64, No. 11, pp. 918-926.*

Tan, F.S.C. (1990) Centrifuge and theoretical modelling of conical footings on sand. *PhD Thesis. Cambridge University, UK.*

Templeton, J.S., Brekke, J.N. and Lewis, D.R. (2005). Spud can fixity in clay, final findings of a study for IADC. *Proc. 10th International Conference of Jack-up Platform, London, UK.*

Templeton, J. S. (2009). Spudcan fixity in clay, further results from a study for IADC. *Proc. 12th International Conference of Jack-up Platform, London, UK.*

Vlahos, G., Cassidy, M.J. and Martin, C.M. (2008). Experimental investigation of the system behaviour of a model three-legged jack-up on clay. *Applied Ocean Research, Vol. 30, No. 4, pp. 323-337.*

Wang, D., Bienen, B., Nazem, M., Tian, Y., Zheng, J., Pucker, T. and Randolph, M.F. (2015). Large deformation finite element analyses in geotechnical engineering. *Computers and Geotechnics, Vol. 65, pp. 104-114.*

Wang, D. and Bienen, B. (2016). Numerical investigation of penetration of a large-diameter footing into normally consolidated kaolin clay with a consolidation phase. *Géotechnique, DOI: http://dx.doi.org/10.1680/jgeot.15.P.048*

Yang, Y., Lee, F.H., Goh, S.H., Zhang, X.Y. and Wu, J.F. (2014). Centrifuge model study of the response of spudcan with lattice leg to rocking. *Proc. 8th International Conference on Physical Modelling in Geotechnics (ICPMG), Perth, Australia, pp. 545-551.*

Yi, J.T., Zhao, B., Li, Y.P., Yang, Y., Lee, F.H., Goh, S.H. & Wu, J.F. (2014). Post-installation pore-pressure changes around spudcan and long-term spudcan behaviour in soft clay. *Computers and Geotechnics, Vol. 56, pp. 133-147.*

Zhang, Y., Bienen, B., Cassidy, M.J. and Gourvenec, S. (2011). The undrained bearing capacity of a spudcan foundation under combined loading in soft clay. *Marine Structures, Vol. 24, No.4, pp. 459-477.*

Zhang, Y., Bienen, B. and Cassidy, M.J. (2013). Development of a combined VHM loading apparatus for a geotechnical drum centrifuge. *International Journal of Physical Modelling in Geotechnics, Vol. 13, No.1, pp. 13-30.*

Zhang, Y., Cassidy, M.J. and Bienen, B. (2014a). A plasticity model for spudcan foundations in soft clay. *Canadian Geotechnical Journal,Vol. 51, No. 6, pp. 629-646.*

Zhang, Y., Wang, D., Cassidy, M.J. and Bienen, B. (2014b). Effect of installation on the bearing capacity of a spudcan under combined loading in soft clay. *Journal of Geotechnical and Geoenvironmental Engineering, Vol. 140, No.7, 04014029.*

LIST OF TABLES

Table 1: Hypoplastic model parameters for Laminaria carbonate silty clay

Table 2: Yield surface parameters for soft normally consolidated clay (Zhang et al. 2014a) at $w/D = 1$. Percentage increases refer to corresponding numerical or experimental $T = 0$ case

Table 3: Percentage increase in H/V_0 and M/DV_0 for pure translation and rotation tests shown in Figures 7, 8

Table 4: Summary of swipe tests simulated numerically and experimentally

LIST OF FIGURES

Figure 1: Three dimensional yield surface and its expansion due to consolidation

Figure 2: bi-logarithmic compression law for structured clays

Figure 3: Spudcan geometry and load-displacement convention

Figure 4: Mesh density and soil domain dimensions

Figure 5: Results of mapping a) excess pore pressure, b) sensitivity, c) void ratio, from two- (LHS) to three-dimensional (RHS) analyses

Figure 6: Load-penetration curves at increasing depth w/D = 1.0; 1.5; 2 showing the effects on further spudcan penetration of different a) length of consolidation T = 0.001; 0.005; 0.01; 0.05; 0.1; 0.5 at constant q_{cons}/q_{ref} = 1 and b) fraction of load held in consolidation q_{cons}/q_{ref} = 0.5; 0.75; 1.0 at constant T = 0.5

Figure 7: Schematic of increase in yield surface size and V_0 magnitude due to a period of consolidation

Figure 8: Load-displacement curves (u/D - H/V_0) following pure horizontal displacement at increasing T for a) $V = 0.5V_0$ (T = 0); b) $V = 0.75V_0$ (T = 0); c) $V = 0.9V_0$ (T = 0)

Figure 9: Moment-rotation curves ($\theta - M/DV_0$) following pure rotation at increasing T for a) $V = 0.5V_0$ (T = 0); b) $V = 0.75V_0$ (T = 0); c) $V = 0.9V_0$ (T = 0)

Figure 10: Comparison of resultant displacement contours following pure horizontal displacement a) without consolidation T = 0; b) including a period of consolidation T = 0.05

*: Zhang et al. (2011) inset not in scale

Figure 11: Comparison of resultant displacement contours following pure rotation a) without consolidation $T = 0$; b) including a period of consolidation $T = 0.05$

*: Zhang et al. (2011) inset not in scale

Figure 12: Void ratio distribution a) without consolidation and b) with consolidation $T = 0.05$

Figure 13: Comparison of excess pore pressure contours following pure horizontal displacement a) without consolidation $T = 0$; b) including a period of consolidation $T = 0.05$

Figure 14: Comparison of excess pore pressure contours following pure rotation a) without consolidation $T = 0$; b) including a period of consolidation $T = 0.05$

Figure 15: Results from numerical simulation of swipe tests in the normalised Q/V_0-V/V_0 plane for increasing consolidation a) $T = 0$; b) $T = 0.01$; c) $T = 0.05$

Figure 16: Sections of the yield surfaces obtained with numerical simulation in the normalised H/V_0-M/DV_0 plane for increasing $V = 0.5$; 0.75; 0.9 V_0 (or V_0^*) and consolidation a) $T = 0$; b) $T = 0.01$; c) $T = 0.05$

Figure 17: Results from experimental swipe tests in the normalised Q/V_0-V/V_0 plane for increasing consolidation a) $T = 0$; b) $T = 0.01$; c) $T = 0.05$

TABLES

Basic Model Parameters				
φ_c	N	λ^*	κ^*	v
CS friction angle	NCL for p'=1 kPa	NCL slope	Unloading-reloading slope	Control on shear modulus
34°	1.697	0.114	0.013	0.1

Other Parameters				
s_{ini}	k	A	s_f	O_c
Initial sensitivity	sensitivity degradation rate	Vol/shear strains effect	Final sensitivity	CSL position
2.9	0.05	0.2	1	1.5

Table 1: Hypoplastic model parameters for Laminaria carbonate silty clay

T	$h_{0,\,num}$	$h_{0,\,exp}$	$m_{0,\,num}$	$m_{0,\,exp}$	e_s	χ
0 (Zhang et al. 2014a)	-	0.198	-	0.092	0.244	0.6
0	0.297	0.186	0.147	0.075	0.1	0.5
0.01	0.309 (+4.0%)	0.215 (+15.6%)	0.151 (+2.7%)	0.085 (+13.3%)	0.1	0.5
0.05	0.387 (+30.3%)	0.268 (+44.1%)	0.152 (+3.4%)	0.089 (+18.6%)	0.1	0.5

Table 2: Yield surface parameters for soft normally consolidated clay (Zhang et al. 2014a) at w/D = 1. Percentage increases refer to corresponding numerical or experimental T = 0 case

		Increase (%)		
V/V_0	Test	T=0	T=0.01	T=0.05
0.5	u (H)	N/A	22.6%	52.9%
	θ (M)	N/A	14.3%	43.0%
0.75	u (H)	N/A	32.2%	69.6%
	θ (M)	N/A	20.7%	56.3%
0.9	u (H)	N/A	37.3%	79.1%
	θ (M)	N/A	32.0%	77.4%

Table 3: Percentage increase in H/V_0 and M/DV_0 for pure translation and rotation tests shown in Figures 7, 8

Swipe Tests (ST)							
Name	***u* (mm)**	***u'*$_{exp}$ (mm/s)**	***θ* (°)**	***θ'*$_{exp}$ (°/s)**	***u*/*Dθ* (-)**	**Num *T***	**Exp *T***
ST1	12	0.4	0	0	∞	0; 0.01; 0.05	0; 0.01; 0.05
ST2	6	0.4	6	0.4	0.95	0; 0.01; 0.05	0; 0.05
ST3	-0.6	-0.04	6	0.4	-0.095	0; 0.01; 0.05	0; 0.05
ST4	0	0	6	0.4	0	0; 0.01; 0.05	0; 0.01; 0.05
ST5	-3.6	-0.24	6	0.4	-0.57	0; 0.01; 0.05	0.05
ST6	-7.2	N/A	6	N/A	-1.14	0; 0.01; 0.05	N/A

Table 4: Summary of swipe tests simulated numerically and experimentally

FIGURES

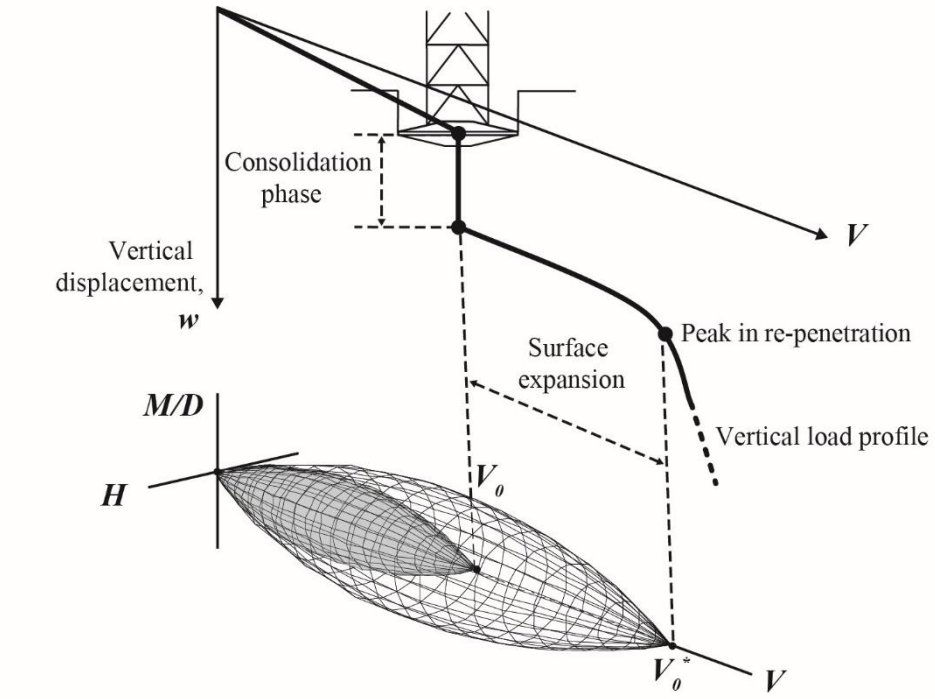

Figure 1: Three dimensional yield surface and its expansion due to consolidation

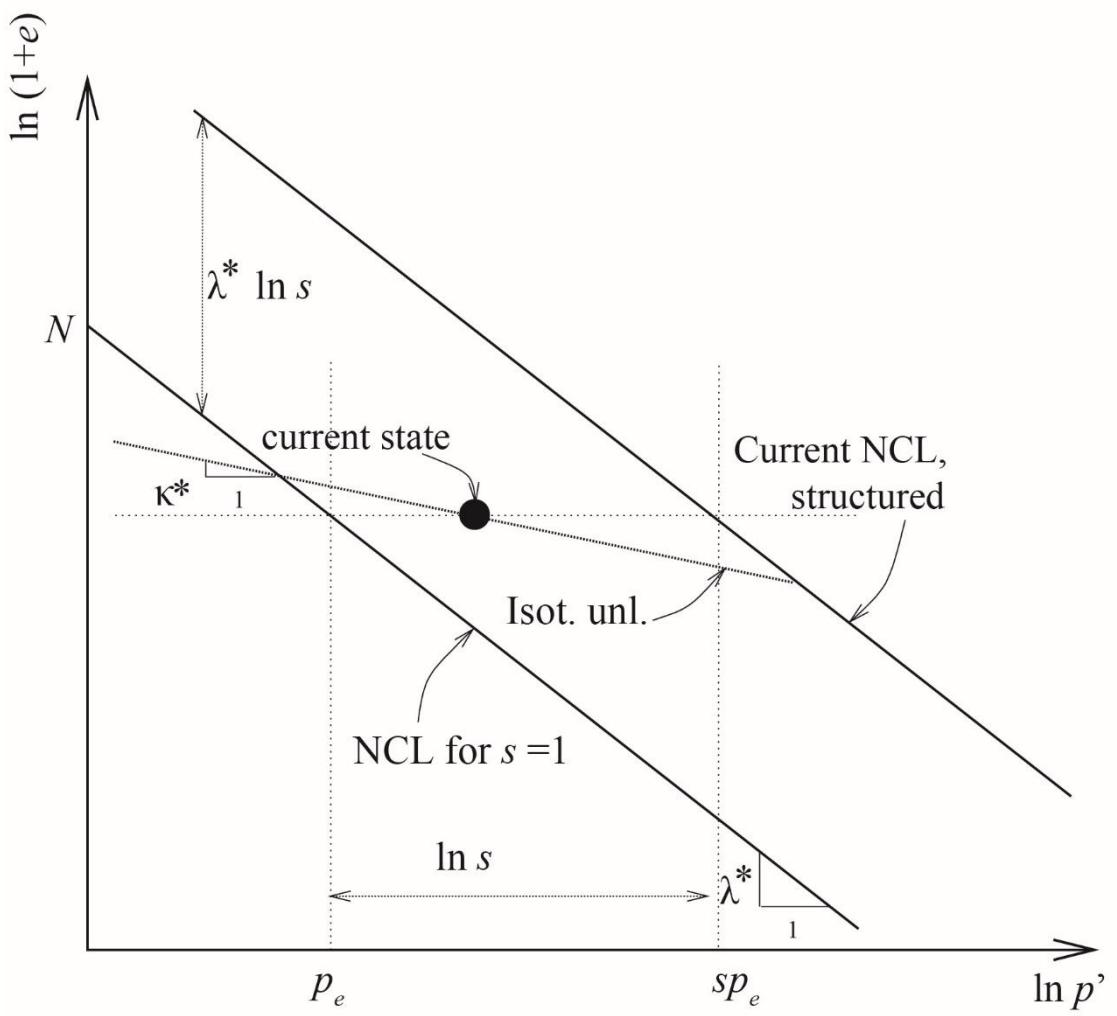

Figure 2: bi-logarithmic compression law for structured clays

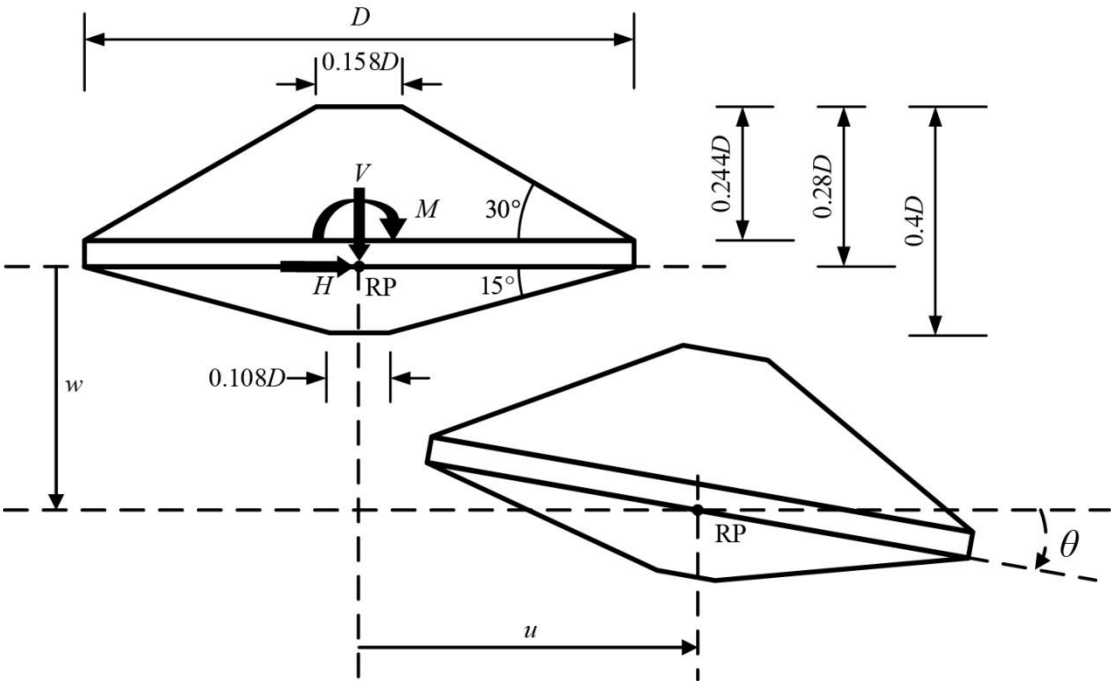

Figure 3: Spudcan geometry and load-displacement convention

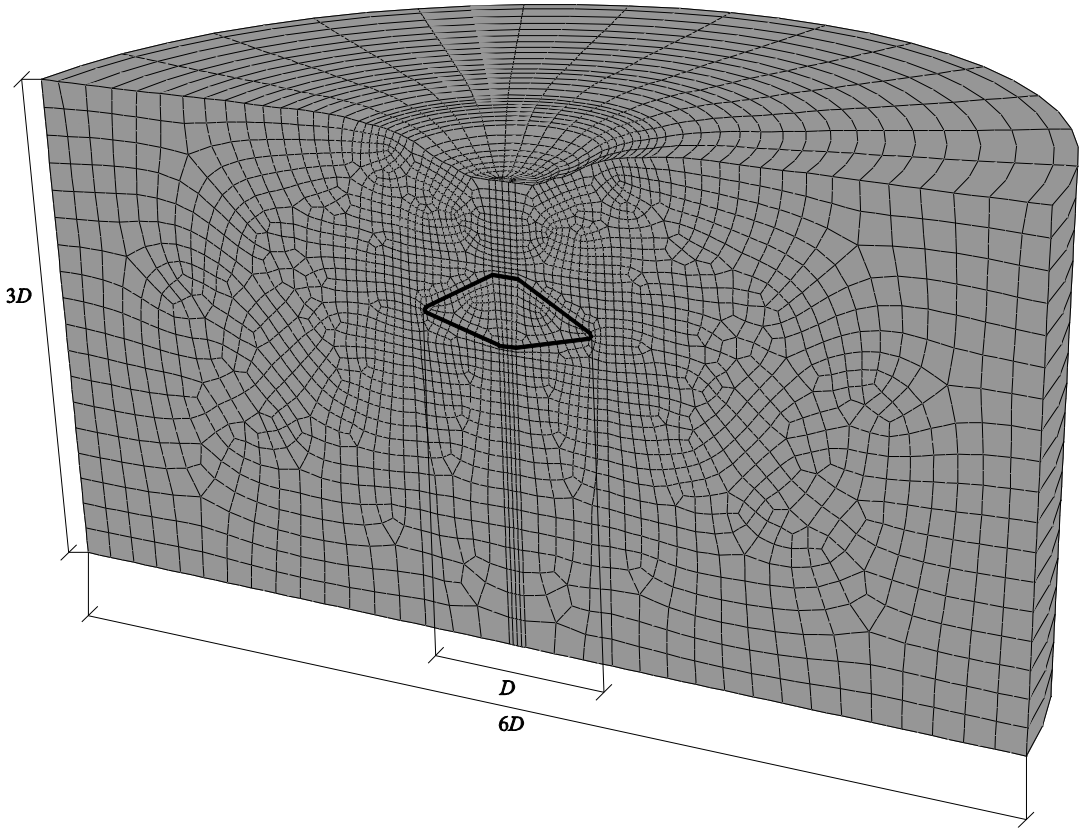

Figure 4: Mesh density and soil domain dimensions

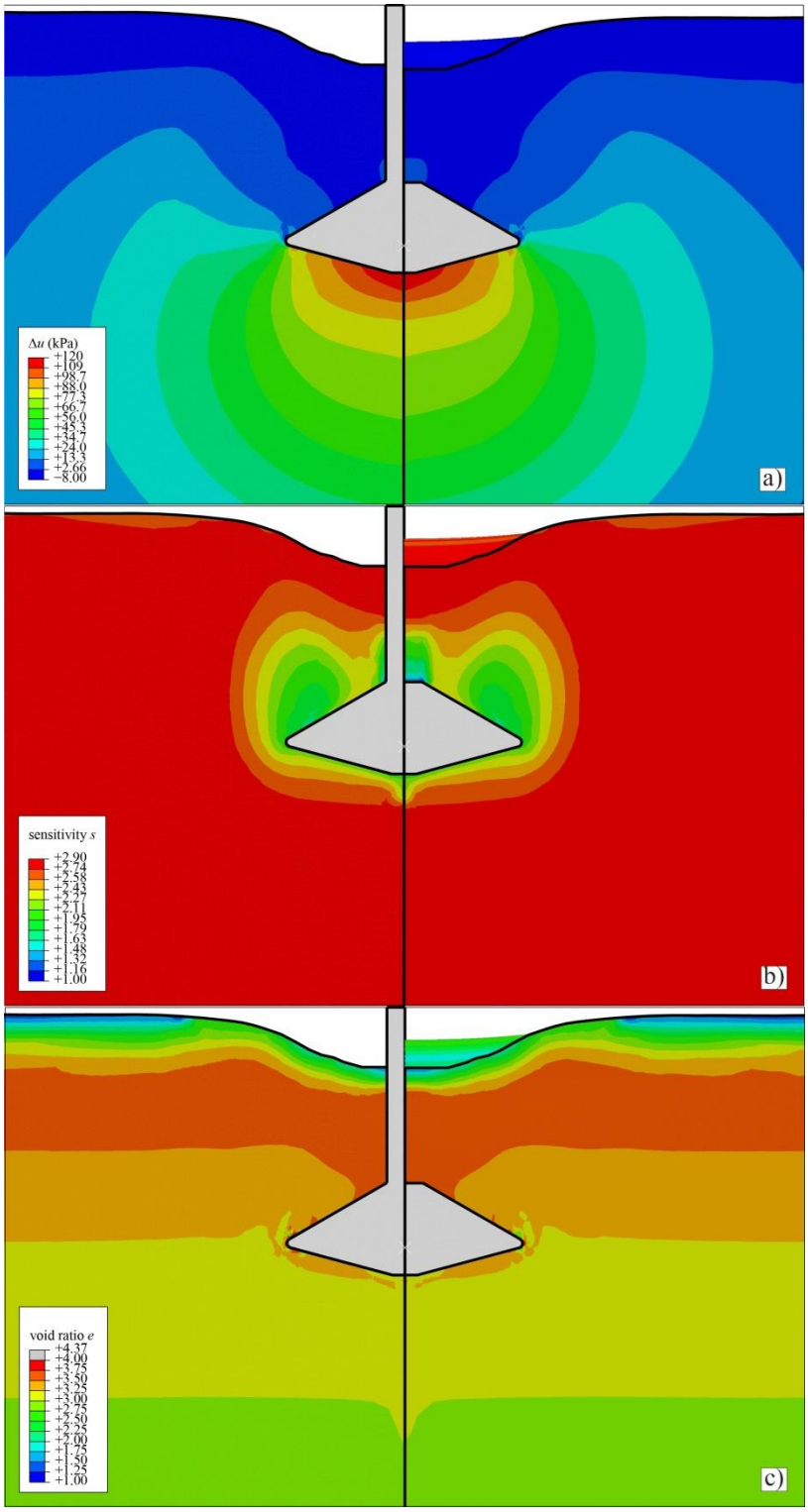

Figure 5: Results of mapping a) excess pore pressure; b) sensitivity; c) void ratio; from two- (LHS) to three-dimensional (RHS) analyses

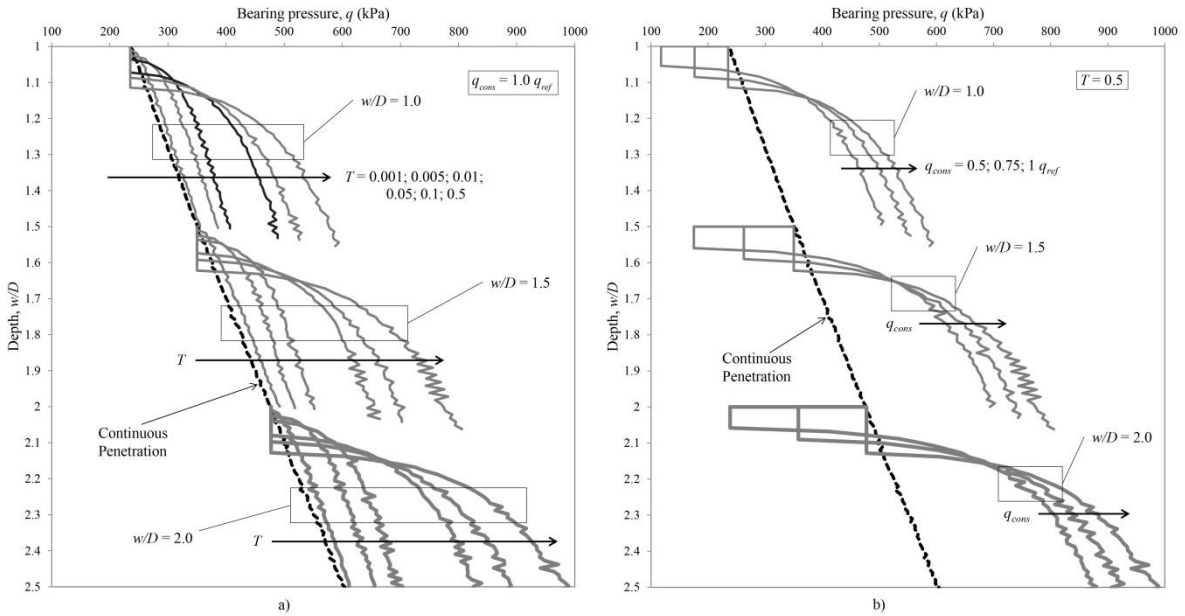

Figure 6: Load-penetration curves at increasing depth w/D = 1.0; 1.5; 2 showing the effects on further spudcan penetration of different a) length of consolidation T = 0.001; 0.005; 0.01; 0.05; 0.1; 0.5 at constant q_{cons}/q_{ref} = 1 and b) fraction of load held in consolidation q_{cons}/q_{ref} = 0.5; 0.75; 1.0 at constant T = 0.5

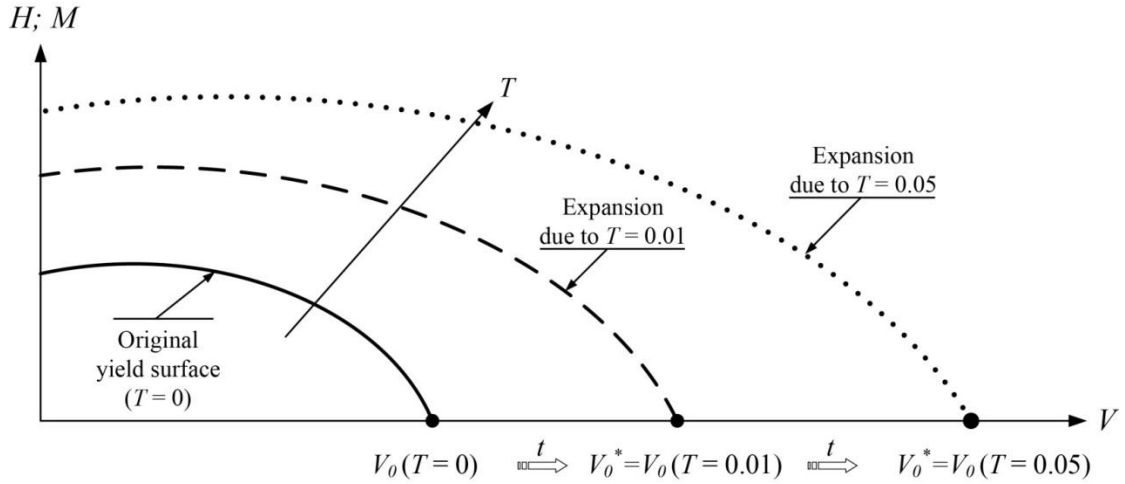

Figure 7: Schematic of increase in yield surface size and V_0 magnitude due to a period of consolidation

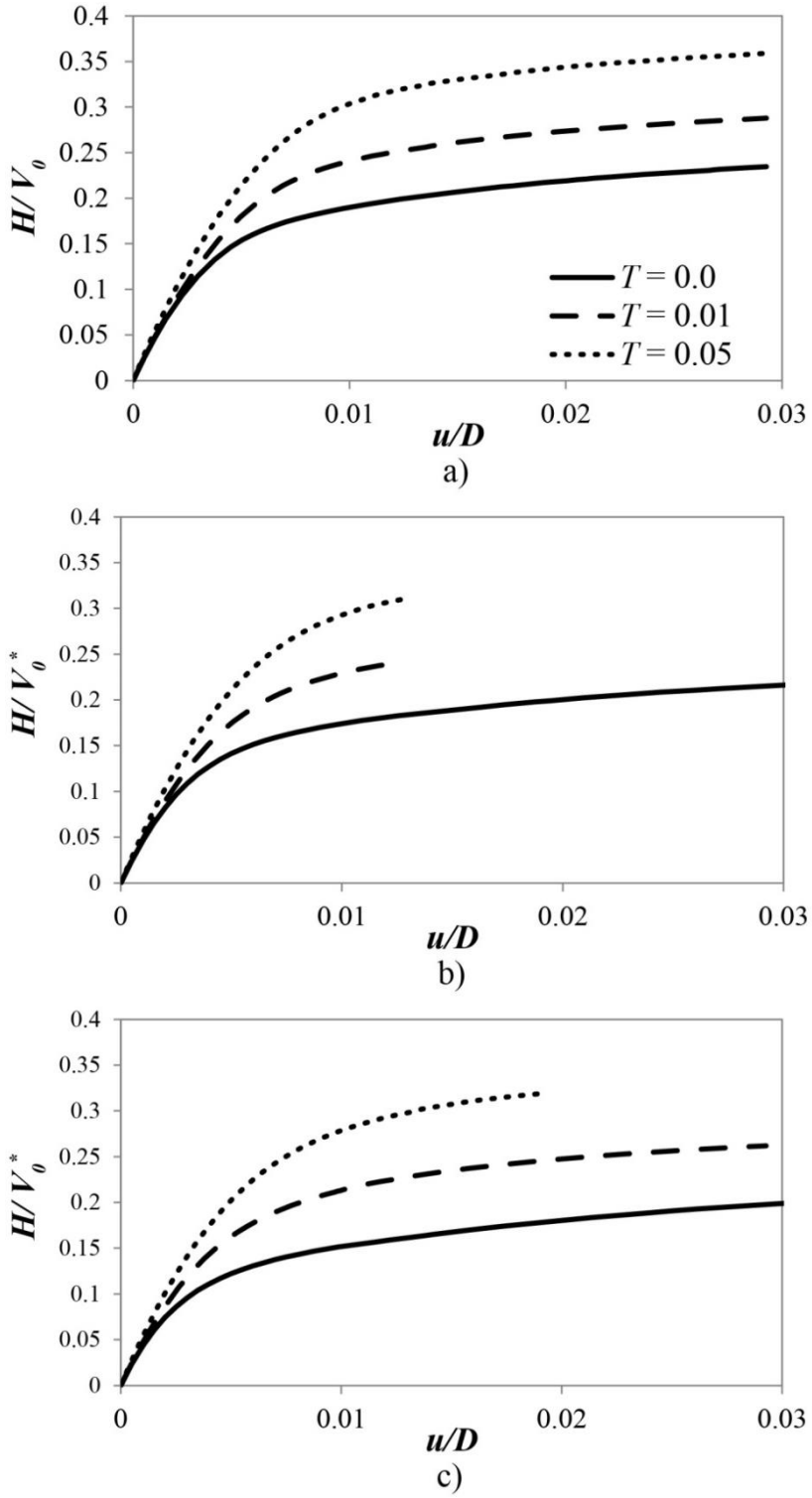

Figure 8: Load-displacement curves (u/D - H/V_0) following pure horizontal displacement at increasing T for a) $V = 0.5V_0$ ($T = 0$); b) $V = 0.75V_0$ ($T = 0$); c) $V = 0.9V_0$ ($T = 0$)

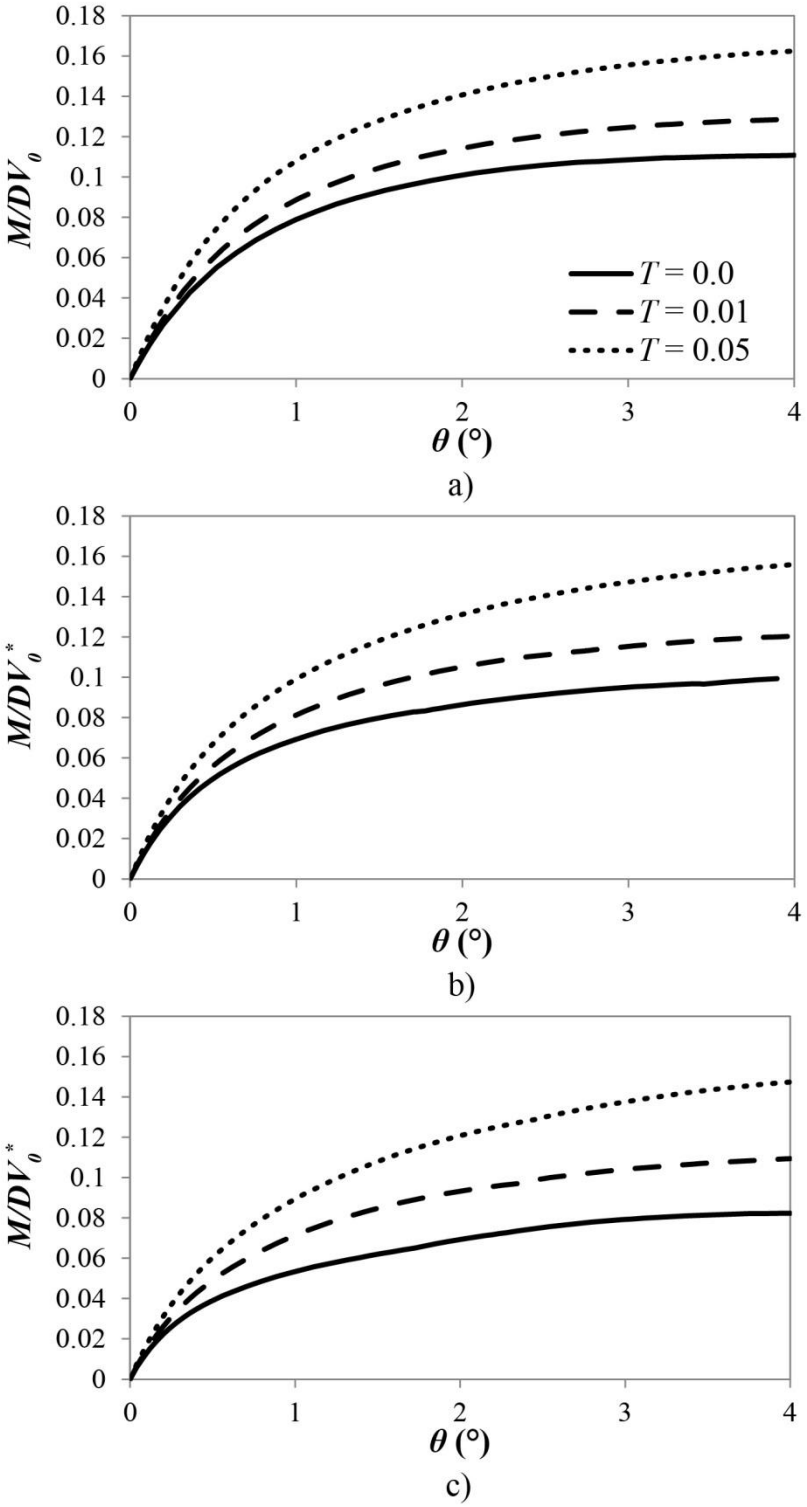

Figure 9: Moment-rotation curves ($\theta - M/DV_0$) following pure rotation at increasing T for a) $V = 0.5V_0$ ($T = 0$); b) $V = 0.75V_0$ ($T = 0$); c) $V = 0.9V_0$ ($T = 0$)

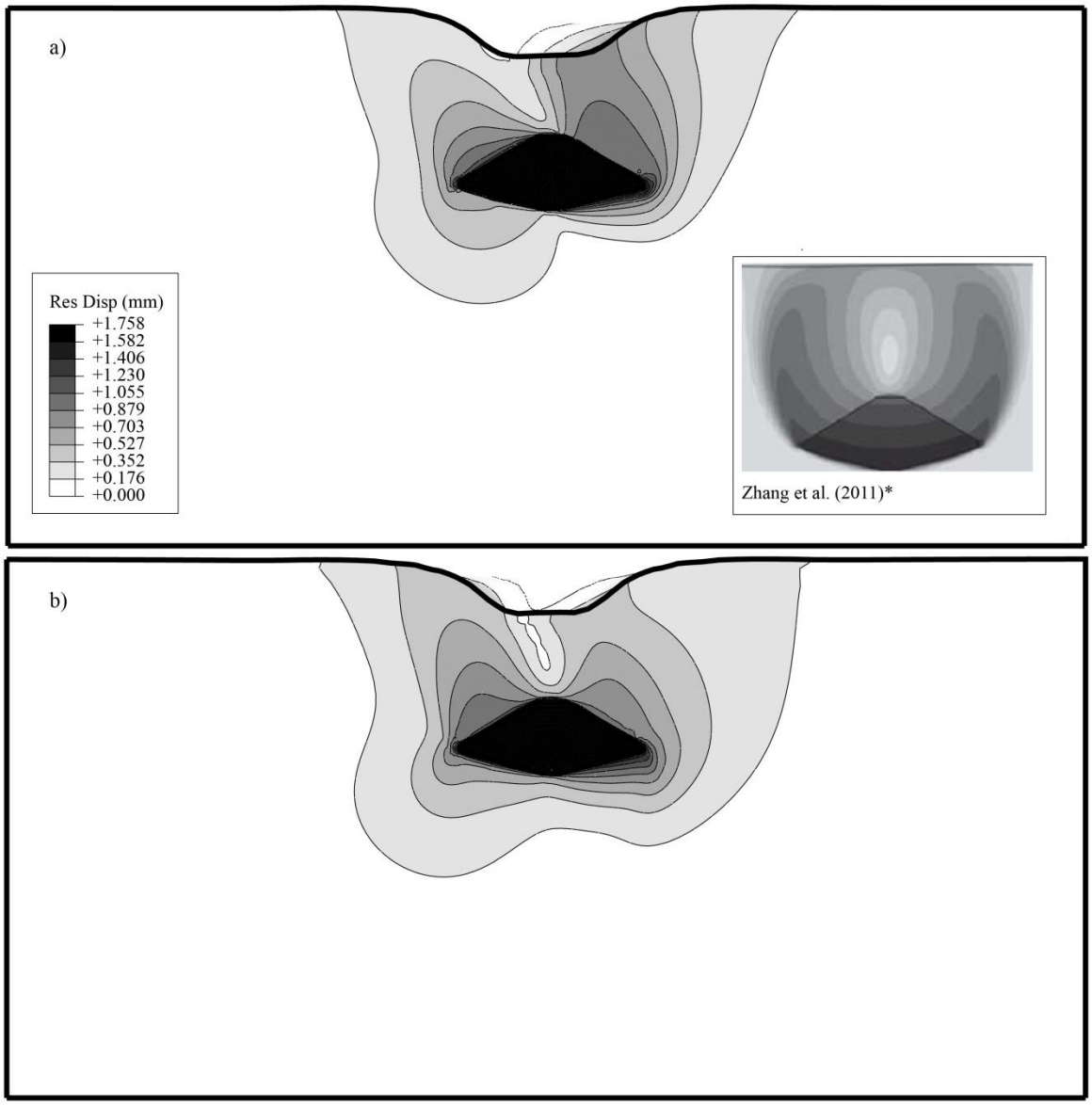

Figure 10: Comparison of resultant displacement contours following pure horizontal displacement a) without consolidation $T = 0$; b) including a period of consolidation $T = 0.05$.

*: Zhang et al. (2011) inset not in scale

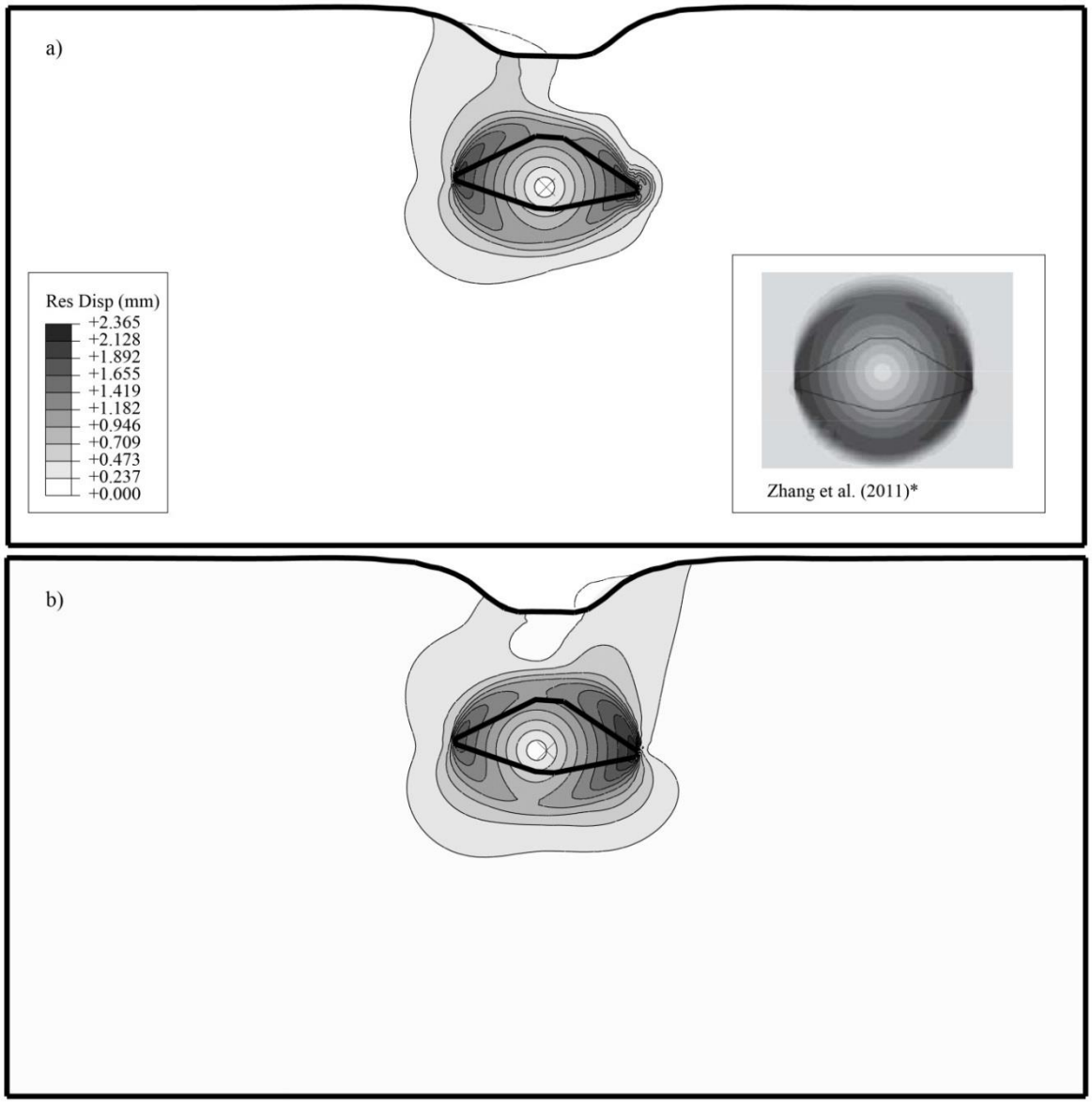

Figure 11: Comparison of resultant displacement contours following pure rotation a) without consolidation $T = 0$; b) including a period of consolidation $T = 0.05$

*: Zhang et al. (2011) inset not in scale

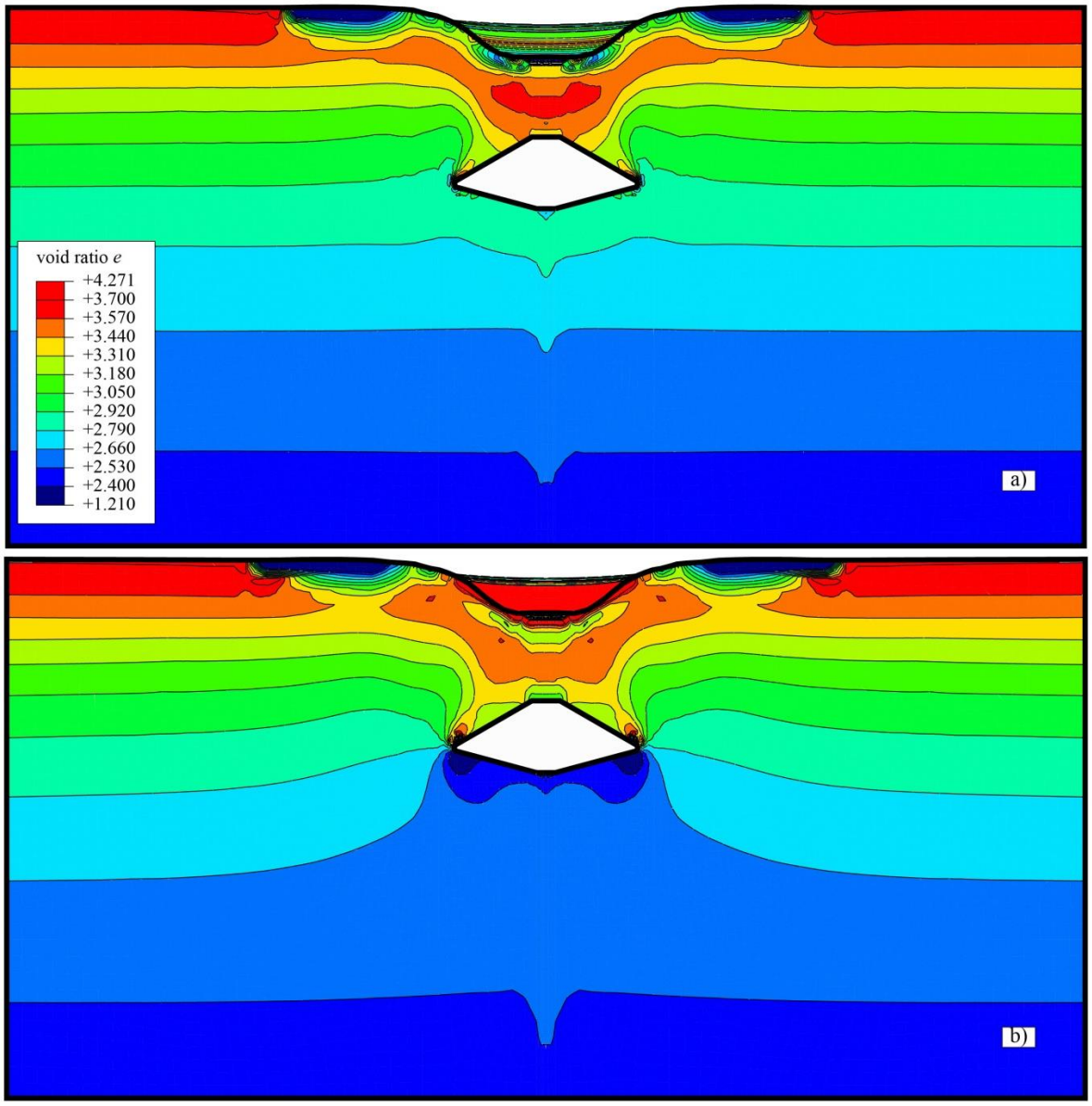

Figure 12: Void ratio distribution a) without consolidation and b) with consolidation $T = 0.05$

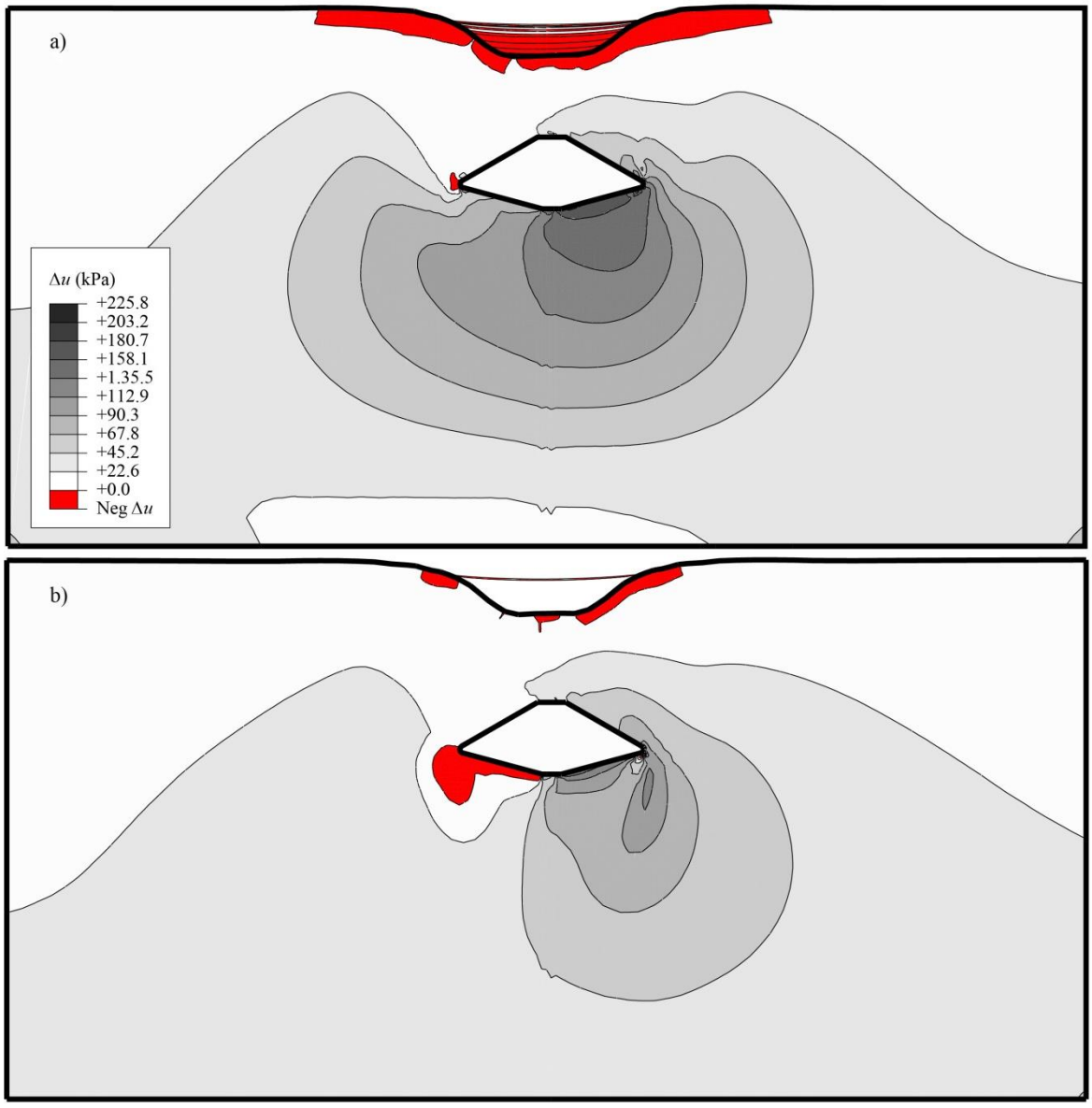

Figure 13: Comparison of excess pore pressure contours following pure horizontal displacement a) without consolidation $T = 0$; b) including a period of consolidation $T = 0.05$

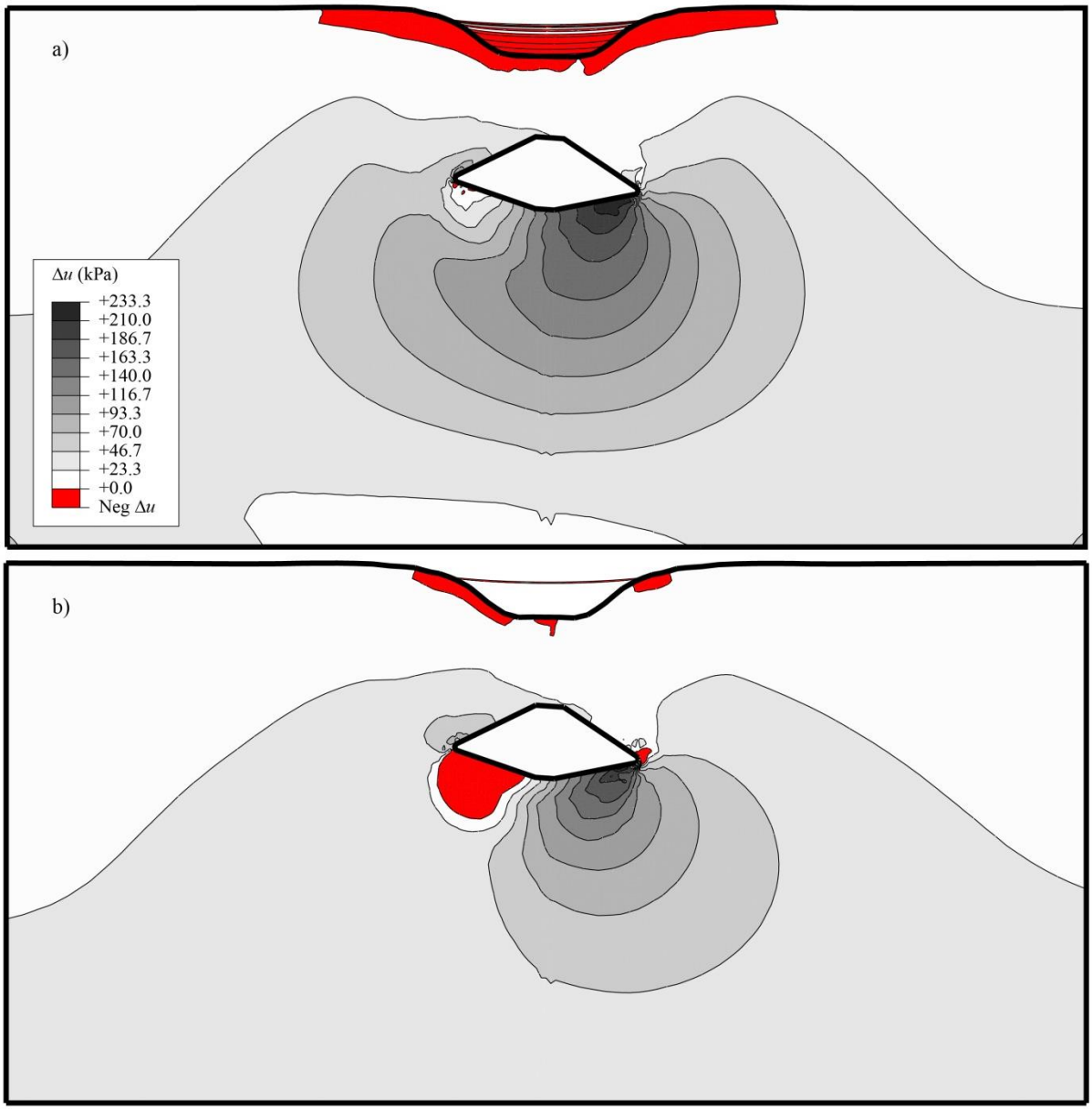

Figure 14: Comparison of excess pore pressure contours following pure rotation a) without consolidation $T = 0$; b) including a period of consolidation $T = 0.05$

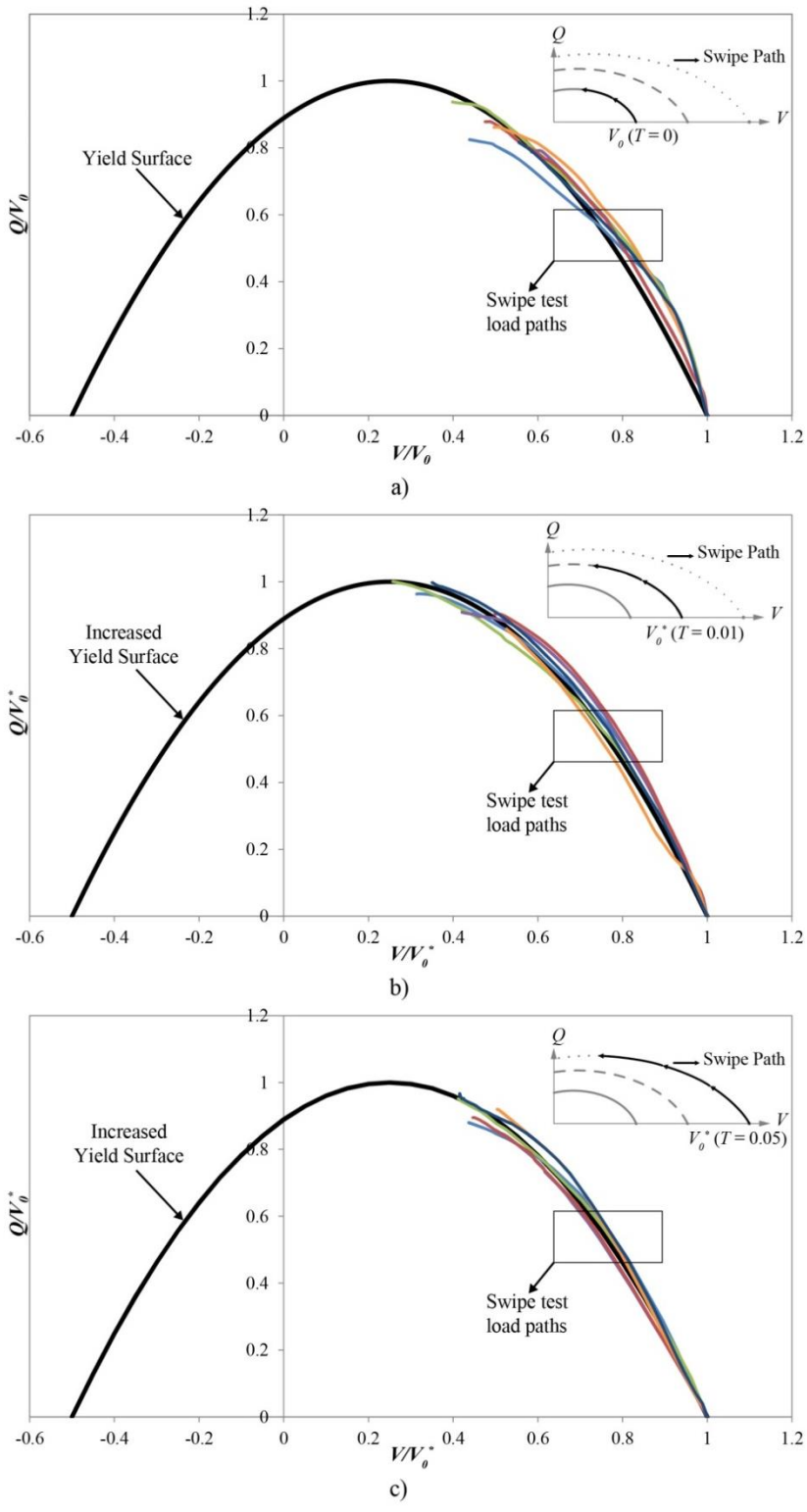

Figure 15: Results from numerical simulation of swipe tests in the normalised Q/V_0-V/V_0 plane for increasing consolidation a) $T = 0$; b) $T = 0.01$; c) $T = 0.05$

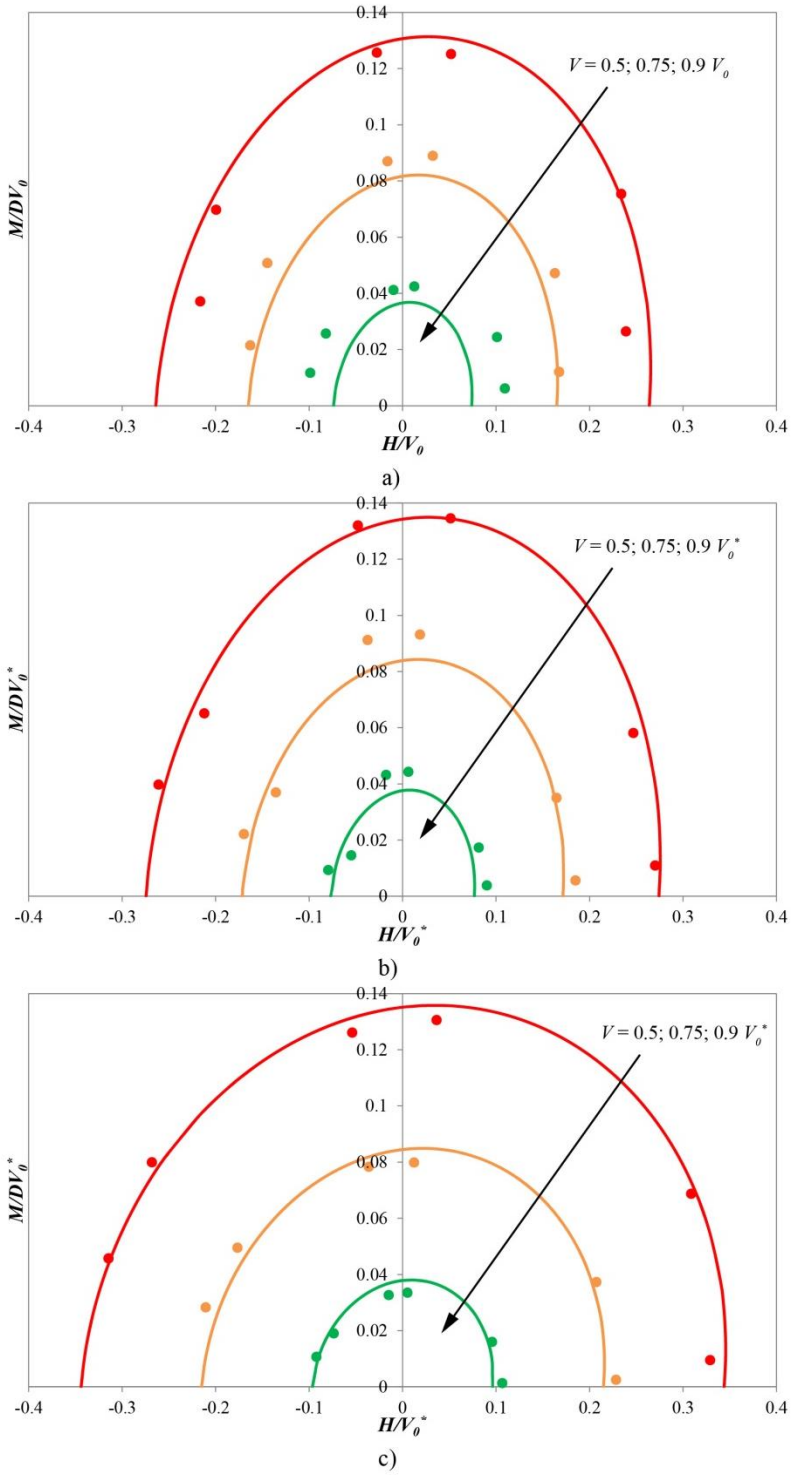

Figure 16: Sections of the yield surfaces obtained with numerical simulation in the normalised H/V_0-M/DV_0 plane for increasing V = 0.5; 0.75; 0.9 V_0 (or V_0^*) and consolidation a) T = 0; b) T = 0.01; c) T = 0.05

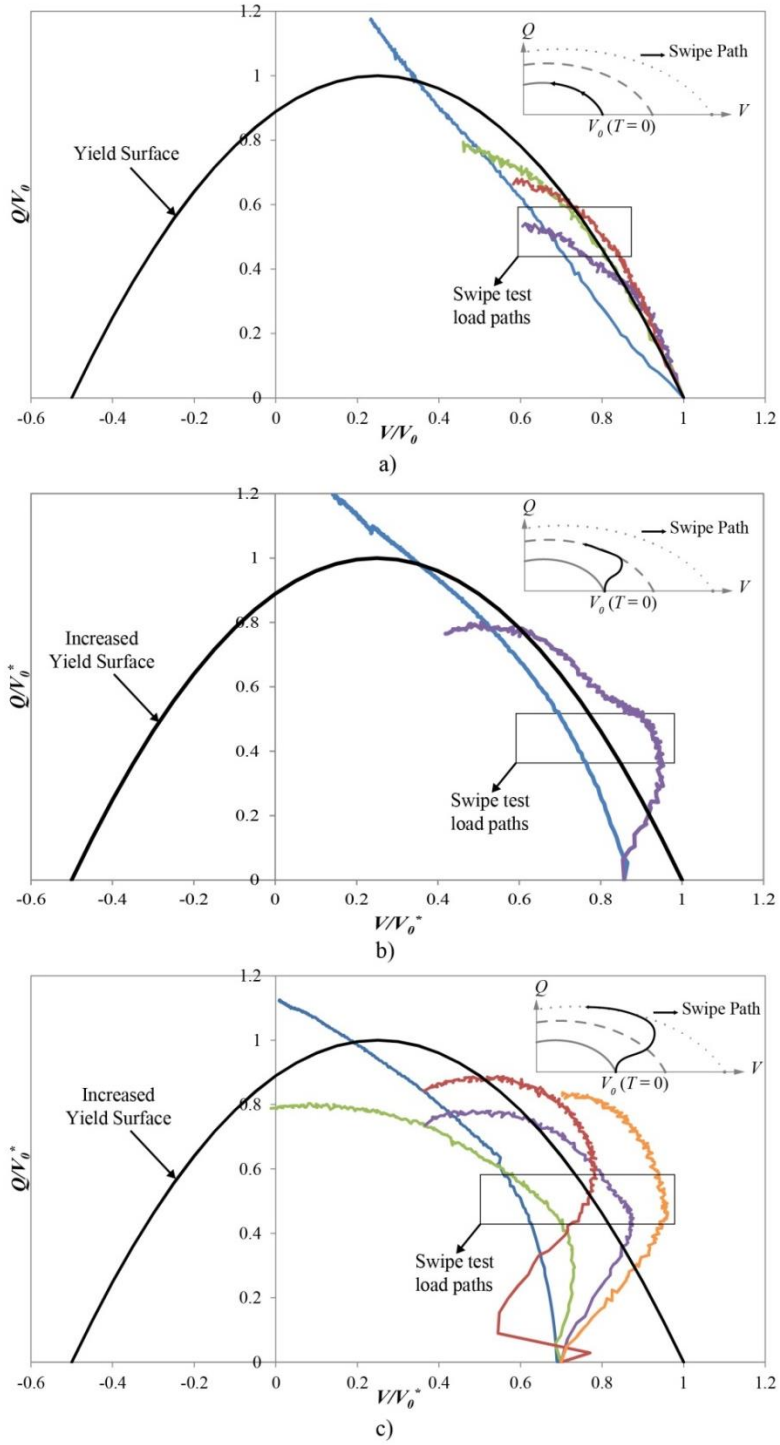

Figure 17: Results from experimental swipe tests in the normalised Q/V_0-V/V_0 plane for increasing consolidation a) $T = 0$; b) $T = 0.01$; c) $T = 0.05$